arXiv:1610.07153v1 [math.NA] 23 Oct 2016

Convex Splitting Method for the Calculation of Transition States of Energy Functional

Shuting Gu [1], Xiang Zhou [2]

Department of Mathematics
City University of Hong Kong
Tat Chee Ave, Kowloon
Hong Kong SAR

ABSTRACT

Among numerical methods for partial differential equations arising from steepest descent dynamics of energy functionals (e.g., Allen-Cahn and Cahn-Hilliard equations), the convex splitting method is well-known to maintain unconditional energy stability for a large time step size. In this work, we show how to use the convex splitting idea to solve the problem of finding transition states, i.e., index-1 saddle points of the same energy functionals. Based on the previous work of iterative minimization formulation (IMF) for saddle points (SIAM J. Numer. Anal., vol. 53, p1786, 2015), we introduce the convex splitting idea to minimize the auxiliary functional at each cycle of the IMF. We present a general principle of constructing convex splitting forms for these auxiliary functionals and show how to avoid solving nonlinear equations. The new numerical scheme based on the convex splitting method allows for a much larger time step size than a traditional semi-implicit scheme we tested and it turns out that a large time step has a huge advantage in computational efficiency. The new methods are tested numerically for the one dimensional Ginzburg-Landau energy functional in the search of the Allen-Cahn or Cahn-Hilliard types of transition states.

Keywords: transition state, saddle point, convex splitting method, iterative minimization formulation

Mathematics Subject Classification (2010) Primary 65K05, Secondary 82B05

1. Introduction

For an energy functional, both its local minimizers and its unstable saddle points have important physical meanings for many problems in physics, chemistry, biology and material sciences. The local minimizers correspond to the stable configurations in physical models, and they manifest themselves as steady states of the gradient flow driven by the energy. For the spatially extended systems, these flows appear mathematically as the time-dependent partial differential equations(PDEs). These PDEs reflect the true physical dynamics of relaxations and they also serve as a convenient computational model to calculate the stable steady states. For instance, as the well-known phase separation and transition models, the Allen-Cahn (AC)

[1]email: shutinggu2-c@my.cityu.edu.hk.

[2]email: xiang.zhou@cityu.edu.hk. The research of XZ was supported by the grants from the Research Grants Council of the Hong Kong Special Administrative Region, China (Project No. CityU 11304314, 11304715 and 11337216).

[1] and Cahn-Hillian (CH) [4] equations are the steepest descent dynamics of the Ginzburg-Landau energy functional under L^2 and H^{-1} norms, respectively. Besides the local minima, the other critical points on an energy surface also play crucial roles for certain problems, such as the energy-barrier activated processes which escape from local minima by crossing saddle points. The infrequent hoppings between neighbouring local minima, although randomly, occur in a quite certain style of travelling through transition states. These transition states, as the bottlenecks on the pathways of activated processes, belong to a class of saddle points with index one, i.e., the unstable critical point whose Hessian has only one negative eigenvalue.

In this paper, we are interested in how to find these index-1 saddle points for a given smooth energy functional. The search for transition states, or index-1 saddle points, faces many challenges. A large number of numerical methods have been proposed and developed to address these challenges. There are also many applications of these saddle point search algorithms in computational chemistry and material sciences. Refer to [31, 39] for review of this topic in molecular computation and phase transformations. One class of numerical methods is to search the so-called minimum energy path (MEP) instead of the transition state. The points along an MEP with locally maximal energy value are then index-1 saddle points and the corresponding tangent direction of the MEP is the one-dimensional unstable direction. These path-finding methods include the string method [8, 9] and nudged elastic band method [22, 19]. The other class of methods is to evolve a single state on the potential energy surface. This is essentially about how to define some dynamics on the energy surface that would converge to index-1 saddle points without knowing multiple local minima *a prior*. The intuitive idea of using the softest direction (having a minimal eigenvalue of the Hessian) to invert the force component along this min-mode direction proves very useful ([20, 30]) and it was proposed probably as early as in 1970s in [7, 6]. Many well-known algorithms and softwares such as the dimer method ([17, 23, 38]) or the activation-relaxation techniques ([28, 27, 5]) are based on this minimum-mode-following idea. The name of the dimer method mainly emphasizes the special algorithm of using two beads for calculating the min-mode; the name of the activation-relaxation mainly refers to the idea of using saddle search method to hop between multiple local minima.

The underlying dynamics of these min-mode-following algorithms has been rigorously formulated and analyzed in [10]. This dynamics, with the name "gentlest ascent dynamics" (GAD), simultaneously evolves both a position variable and a direction variable. By analyzing the eigenvalue of the GAD, [10] for the first time rigorously proved the locally linear convergence rate to index-1 saddle point. To accelerate the convergence rate for the GAD, a discrete iterative mapping, named the "iterative minimization formulation" (IMF), has been proposed in [13]. There are three advantageous features of the IMF: (1) it has the quadratic convergence rate for non-degenerate saddle points; (2) it turns the problem of searching unstable saddle points into a series of minimization subproblems; (3) there is no restriction for numerical methods to solve minimization subproblems in the IMF. The only important issue in practice for better efficiency is to use the adaptive stopping rule as an inexact solver in solving these subproblems, which is similar to the augmented Lagrangian method for constrained optimization problems [29]. For a thorough discussion of the practical algorithms based on the IMF, the readers can refer to [14].

The advantages and flexibilities offered by the IMF immediately provide many new opportunities to explore the existing methods which were designed purely for searching local minima. The convex splitting method, originally proposed in [11], successfully gives unconditionally energy stable schemes so that it can ensure a large time step size. The effectiveness of this method in resolving gradient dynamics as well as calculating the minimizers has been demonstrated by a vast number of applications, for example, the phase field model in [12], the phase field crystal model in [35], the thin film epitaxy model in [32], the binary fluid surfactant model in [16], as well as many others ([33, 34, 36, 21]).

In this paper, our motivation is to test the performance of the convex splitting method if this strategy is used to locate the saddle point. As we mentioned earlier, the IMF solves the saddle point search problem by solving a series of minimization subproblems, and these subproblems can be solved by running the steepest decent dynamics. Since the outer iteration of the IMF (referred as "cycle" in [13, 14]) is of quadratic convergence rate and it usually only takes a few cycles in practice to reach the desired accuracy, then one can expect that a better method for the subproblem may gain a better speedup in efficiency. At least, the benefit of adopting the convex splitting idea is that the subproblems can be solved by a very large time step size, or any time step size in principle. When we apply this method to the example of the Ginzburg-Landau energy functional, we observe a significant improvement of the overall efficiency compared, which is the main conclusion we shall report in this article.

The idea of the convex splitting method is quite simple, but there are two important practical issues when applied to specific problems. The first is the construction of a convex splitting form for a given energy functional. In theory([11]), there always exist multiple convex splitting forms for any continuous functional. The explicit decomposition has to be sought for specific problems. The second is that one should try best to construct a *linear* time-implicit term in the convex spitting scheme since this can avoid involving the Newton-type method to solve a nonlinear system at each time step. The existence of such a splitting form with this desired property certainly depends on the specific expression of the energy functional. For the Ginzburg-Landau functional with the double-well potential, the above two tasks have been resolved before in other literature of applying the convex splitting method to the CH equation [12].

The contributions in our work of applying the convex splitting method to saddle point search problems include the following: (1) for any given convex splitting form of the original energy functional, we show how to explicitly obtain the corresponding convex splitting form of the auxiliary functional in the IMF. This means that we design an automatic procedure from the traditional convex splitting method for local minimizers to the convex splitting method for saddle points; (2) we shall see later that the auxiliary functional in the IMF consists of multiple terms involving the original energy functional. By adapting different forms of the convex splitting for different terms in the auxiliary functional, we can ensure the time-explicit discretization for nonlinear terms and obtain a linear system. We demonstrate how to achieve this by the example of Ginzburg Landau energy functional. The condition is that one need know at least one convex splitting form with the time-explicit nonlinear term for the original energy functional. Besides, we also show that in the case of the periodic boundary condition, the IMF still possesses the quadratic

convergence rate, despite of the degeneracy arising from the spatial translation invariance. This is an important conclusion because the quadratic convergence rate is the cornerstone of our method. The proof is presented in the appendix.

The rest of the paper is organized as follows. In Section 2, we review the IMF for the saddle point search problem and the convex splitting method. In Section 3, we construct the convex splitting method for saddle point search problems and discuss numerical issues. Section 4 presents the detailed numerical schemes and substantial numerical results for the Ginzburg Landau energy functional in the L^2 and H^{-1} metric, respectively, subject to the Neumann or periodic boundary condition. The conclusion is drawn in Section 5.

2. Review

In this section, we review two foundations of our method, which were born apparently from two different areas.

2.1. The IMF for the saddle point search.

We first recall the IMF [13] which aims to locate the saddle point of a potential function by solving a series of minimization subproblems.

Let $\mathcal{M}$ be a Hilbert space equipped with the norm $\|\cdot\|$ and the inner product $\langle\cdot,\cdot\rangle$. Suppose that $V(x):\mathcal{M}\to\mathbb{R}$ is a sufficiently smooth potential function, then the IMF is the following iteration for the position variable x and the direction variable v

$$\begin{cases} v^{(k+1)} = \underset{\|u\|=1}{\operatorname{argmin}} \left\langle u, H(x^{(k)})u \right\rangle, & (2.1)\\ x^{(k+1)} = \underset{y}{\operatorname{argmin}}\, L(y; x^{(k)}, v^{(k+1)}), & (2.2) \end{cases}$$

where

$$H(x^{(k)}) = \nabla^2 V(x^{(k)}),$$

and

$$\begin{aligned} L(y; x^{(k)}, v^{(k+1)}) = (1-\alpha)V(y) &+ \alpha V\left(y - (v^{(k+1)}\otimes v^{(k+1)})(y-x^{(k)})\right)\\ &- \beta V\left(x^{(k)} + (v^{(k+1)}\otimes v^{(k+1)})(y-x^{(k)})\right). \end{aligned} \tag{2.3}$$

α and β are two parameters and $\alpha+\beta>1$. Two special choices for α and β are: (i) $(\alpha,\beta)=(2,0)$, then $L(y;x,v)=-V(y)+2V(y-v\otimes v(y-x))$; (ii) $(\alpha,\beta)=(0,2)$, then $L(y;x,v)=V(y)-2V(x+v\otimes v(y-x))$. The main properties of the auxiliary objective function $L(y;x,v)$ when $\alpha+\beta>1$ are listed here for reference.

Theorem 1. [13] *Suppose that x^* is a (non-degenerate) index-1 saddle point of a C^4-function $V(x)$, i.e., its all eigenvalues are $\lambda_1<0<\lambda_2\le\cdots$, and the auxiliary function L is defined by (2.3) with $\alpha+\beta>1$, then*
(1) *there exists a neighbourhood $\mathcal{U}$ of x^* such that for any $x\in\mathcal{U}$, $L(y;x,v)$ is strictly convex in $y\in\mathcal{U}$ and thus has a unique minimum in $\mathcal{U}$;*
(2) *define the mapping $\Phi: x\in\mathcal{U}\to\Phi(x)\in\mathcal{U}$ to be the unique local minimizer of L in $\mathcal{U}$ for any $x\in\mathcal{U}$. Further assume that $\mathcal{U}$ contains no other stationary points of V except for x^*. Then the mapping Φ has only one fixed point x^*;*
(3) *the mapping $x\to\Phi(x)$ has a quadratic convergence rate.*

The IMF includes two-level iterations. The top level is the IMF mapping $x \to \Phi(x)$, referred as "cycle". The k-th cycle means the step of $x^{(k)} \to x^{(k+1)} = \Phi(x^{(k)})$, which in practice consists of a second-level iterative procedure to solve (2.1) for the min-mode (the so-called "rotation step") and (2.2) to update the position("translation step"). The rotation step is a classical numerical eigenvector problem, for which many methods have been constructed such as the power method ([10]), the conjugate gradient method([18, 20]), the Lanczos algorithm([28, 27, 5]) and the state-of-the-art LOR in [24], etc. The readers can also refer to the refer-ecence [37]. The translation step in the IMF is actually a minimization problem and it is not exactly the same as the traditional translation step in the dimer-type methods which is just a single movement ([14]). In this paper, we do not delve into the rotation step and only focus on the subproblem (2.2) of minimizing the auxiliary function.

We are interested in spatially extended systems, i.e., $\mathcal{M}$ is a function space and V is actually a functional on $\mathcal{M}$. As a convention, we use $F(\phi)$ rather than $V(x)$ below to represent the functional of a spatial function ϕ.

2.2. **Convex splitting method.** Let $\phi(x,t) : [0,1] \times \mathbb{R}^+ \to \mathbb{R}$ be the solution of the following PDE driven by the gradient flow

$$\frac{\partial \phi}{\partial t} = -\frac{\delta F}{\delta \phi}(\phi), \tag{2.4}$$

subject to certain boundary condition at $x = 0$ and 1. F is a sufficiently smooth free energy functional bounded from below. $\frac{\delta F}{\delta \phi}$ is the first order variational derivative of $F(\phi)$ with respect to ϕ. A convex splitting form of $F(\phi)$ means that there exist two convex functionals, denoted by F_c and F_e, such that

$$F(\phi) = F_c(\phi) - F_e(\phi), \tag{2.5}$$

where "c" refers to the contractive part of the energy and "e" refers to the expansive part ([11]). Then the convex splitting scheme for (2.4) is

$$\frac{\phi^{n+1} - \phi^n}{\Delta t} = -\left(\frac{\delta F_c}{\delta \phi}\left(\phi^{n+1}\right) - \frac{\delta F_e}{\delta \phi}\left(\phi^n\right) \right), \tag{2.6}$$

where $\phi^n \approx \phi(t_n)$ is the numerical solution at the n-th time level $t_n = n\Delta t$ and Δt is the time step size. In this scheme, the force from contractive part is time-implicit and the force from the expansive part is time-explicit. The time-discrete scheme (2.6) has the property of the so-called unconditional energy stability, as stated in the following theorem.

Theorem 2 ([35]). *Suppose the free energy functional $F(\phi)$ can be split into two parts $F(\phi) = F_c(\phi) - F_e(\phi)$ as in (2.5). Then the time-discrete scheme (2.6) is unconditionally energy stable, meaning that for any time step size $\Delta t > 0$,*

$$F(\phi^{n+1}) \le F(\phi^n), \quad n = 0, 1, 2, \cdots.$$

The convexity of F_c and F_e do not have to be valid in the whole real line. In practical applications, it only requires the convexity over a finite interval where the solution ϕ always stays.

3. Main method

We consider the 1-D spatial domain $(0,1)$. The high dimensional case follows exactly the same idea. Let $\mathcal{M}$ be a function space on the interval $[0,1]$. For example, $\mathcal{M}$ is the Hilbert space $H^1([0,1])$ or some other subspaces of $L^2([0,1])$. In this paper, we illustrate our idea by using a specific example: the Ginzburg-Landau energy functional F on $\mathcal{M}$,

$$F(\phi) = \int_0^1 \frac{\kappa^2}{2}|\phi_x|^2 + f(\phi(x))\,dx, \qquad \phi \in \mathcal{M},$$

where $f(\phi) = (\phi^2-1)^2/4$ is the double-well potential function. The norm in $\mathcal{M}$ is denoted by $\|\cdot\|$ and the inner product is denoted by $\langle\cdot,\cdot\rangle$.

Assume that the second order variational derivative of F in $\mathcal{M}$ exists. We rewrite the IMF in Section 2.1 in $\mathcal{M}$:

$$\begin{cases} v^{(k+1)} = \underset{\|v\|=1}{\operatorname{argmin}} \left\langle v, H(\phi^{(k)})v \right\rangle, & (3.1) \\ \phi^{(k+1)} = \underset{\phi}{\operatorname{argmin}}\, L(\phi;\phi^{(k)},v^{(k+1)}), & (3.2) \end{cases}$$

where $H(\phi) := \frac{\delta^2 F(\phi)}{\delta\phi^2}$ is the second order variational operator of $F(\phi)$ and the auxiliary functional L is constructed with the following expression

$$L(\phi;\phi^{(k)},v^{(k+1)}) = F(\phi) - \alpha F(\phi) + \alpha F(\phi - \tilde{\phi}) - \beta F(\phi^{(k)} + \tilde{\phi}), \tag{3.3}$$

where we define

$$\tilde{\phi} := (v^{(k+1)} \otimes v^{(k+1)})(\phi - \phi^{(k)}) \tag{3.4}$$

to ease the notation. The min-mode $v^{(k+1)}$ belongs to the tangent space $\mathcal{T}_{\mathcal{M}}$, the tangent space of $\mathcal{M}$. $u \otimes v$ denotes the tensor defined by $(u\otimes v)\phi = \langle v,\phi\rangle\, u$ for $u, v \in \mathcal{T}_{\mathcal{M}}$ (so, in strict sense, $\langle\cdot,\cdot\rangle$ is defined in $\mathcal{T}_{\mathcal{M}}$). We assume $\alpha+\beta > 1$ as before.

3.1. Convex splitting method for minimizing the auxiliary functional L.

We shall approximate the solution of the variational subproblem (3.2)

$$\min_{\phi} L\left(\phi;\, \phi^{(k)}, v^{(k+1)}\right)$$

at the k-th IMF cycle by the steady solution of the gradient flow associated with L,

$$\frac{\partial\phi}{\partial t} = -\frac{\delta L}{\delta\phi}. \tag{3.5}$$

In solving this problem, $\phi^{(k)}$ and $v^{(k+1)}$ are fixed parameters. This solution at infinite time is well-defined if the lowest eigenvalue of $\phi^{(k)}$ is negative ([13, 14]).

Next, we show how to construct the convex splitting scheme for equation (3.5). Our starting point is that one has already been able to solve the gradient flow of the original energy functional F by a convex splitting scheme. This means that a convex splitting form for $F(\phi)$ has been given, say,

$$F(\phi) = F_c(\phi) - F_e(\phi). \tag{3.6}$$

By substituting (3.6) into (3.3), we find the following convex splitting form for L

$$L(\phi;\,\phi^{(k)},v^{(k+1)}) = L_c(\phi;\,\phi^{(k)},v^{(k+1)}) - L_e(\phi;\,\phi^{(k)},v^{(k+1)}), \tag{3.7}$$

where

$$L_c(\phi;\phi^{(k)},v^{(k+1)}) =$$

$$\begin{cases} F_c(\phi)+\alpha F_e(\phi)+\alpha F_c(\phi-\tilde{\phi})+\beta F_e(\phi^{(k)}+\tilde{\phi}), \text{if } \alpha\geq 0,\beta\geq 0; \\ F_c(\phi)+\alpha F_e(\phi)+\alpha F_c(\phi-\tilde{\phi})-\beta F_c(\phi^{(k)}+\tilde{\phi}), \text{if } \alpha\geq 0,\beta\leq 0; \\ F_c(\phi)-\alpha F_c(\phi)-\alpha F_e(\phi-\tilde{\phi})+\beta F_e(\phi^{(k)}+\tilde{\phi}), \text{if } \alpha\leq 0,\beta\geq 0, \end{cases} \tag{3.8}$$

and $L_e(\phi;\phi^{(k)},v^{(k+1)})$ is defined likewise by exchanging F_e and F_c:

$$L_e(\phi;\phi^{(k)},v^{(k+1)}) =$$

$$\begin{cases} F_e(\phi)+\alpha F_c(\phi)+\alpha F_e(\phi-\tilde{\phi})+\beta F_c(\phi^{(k)}+\tilde{\phi}), \text{if } \alpha\geq 0,\beta\geq 0; \\ F_e(\phi)+\alpha F_c(\phi)+\alpha F_e(\phi-\tilde{\phi})-\beta F_e(\phi^{(k)}+\tilde{\phi}), \text{if } \alpha\geq 0,\beta\leq 0; \\ F_e(\phi)-\alpha F_e(\phi)-\alpha F_c(\phi-\tilde{\phi})+\beta F_c(\phi^{(k)}+\tilde{\phi}), \text{if } \alpha\leq 0,\beta\geq 0. \end{cases} \tag{3.9}$$

Note that $\tilde{\phi}$ is already defined in (3.4).

Property 3. *$L_c(\phi;\phi^{(k)},v^{(k+1)})$ and $L_e(\phi;\phi^{(k)},v^{(k+1)})$ defined above are all convex with respect to ϕ for any $\phi^{(k)}$ and any $v^{(k+1)}$.*

Proof. We only prove the case when $\alpha\geq 0,\beta\geq 0$ since the other two cases can be proved similarly. The proofs of the convexity for L_c and L_e are the same, thus it suffices to only show two special terms $F_c(\phi-\tilde{\phi})$ and $F_e(\phi^{(k)}+\tilde{\phi})$ in (3.8) are both convex in terms of ϕ. Denote the second order variational operators of $F_c(\phi)$ and $F_e(\phi)$ by H_c and H_e, respectively, then both H_c and H_e are semi-positive definite by the property of convexity. By the definition of $\tilde{\phi}$ in (3.4), the second order derivatives of $F_c(\phi-\tilde{\phi})$ and $F_e(\phi^{(k)}+\tilde{\phi})$ are

$$[I-(v\otimes v)]H_c(\phi-\tilde{\phi})[I-(v\otimes v)]$$

and

$$(v\otimes v)H_e(\phi^{(k)}+\tilde{\phi})(v\otimes v),$$

respectively, where $v=v^{(k+1)}$. Since v is nonzero, these two (projected) Hessians are also semi-positive definite. This completes our proof. □

After getting the convex splitting form for $L(\phi;\phi^{(k)},v^{(k+1)})$, we now present our time-discrete numerical scheme for (3.5) based on the convex splitting idea in Section 2.2. Here we only consider the case $\alpha\geq 0,\beta\geq 0$. To simplify the notation, we drop out the parameters $\phi^{(k)}$ and $v^{(k+1)}$ in the expressions of $L(\phi,\phi^{(k)},v^{(k+1)})$, $L_c(\phi,\phi^{(k)},v^{(k+1)})$ and $L_e(\phi,\phi^{(k)},v^{(k+1)})$.

Let ϕ^n be the numerical solution at the time level t_n. Our scheme is

$$\frac{\phi^{n+1}-\phi^n}{\Delta t} = -\left[\frac{\delta L_c}{\delta\phi}(\phi^{n+1})-\frac{\delta L_e}{\delta\phi}(\phi^n)\right], \tag{3.10}$$

with initial $\phi^0=\phi^{(k)}$. We caluculate the first order variational derivatives of L_c and L_e from (3.8) ad (3.9):

$$\begin{aligned} \frac{\delta L_c}{\delta\phi}(\phi) =& \frac{\delta F_c}{\delta\phi}(\phi)+\alpha\frac{\delta F_e}{\delta\phi}(\phi) \\ &+\alpha\big(I-(v^{(k+1)}\otimes v^{(k+1)})\big)\frac{\delta F_c}{\delta\phi}\left(\phi-(v^{(k+1)}\otimes v^{(k+1)})(\phi-\phi^{(k)})\right) \\ &+\beta(v^{(k+1)}\otimes v^{(k+1)})\frac{\delta F_e}{\delta\phi}\left(\phi^{(k)}+(v^{(k+1)}\otimes v^{(k+1)})(\phi-\phi^{(k)})\right), \end{aligned}$$

and $\frac{\delta L_e}{\delta \phi}(\phi)$ is defined likewise by switching $\frac{\delta F_c}{\delta \phi}(\phi)$ and $\frac{\delta F_e}{\delta \phi}(\phi)$ in the above expression.

For the same reason in Theorem 2, the following unconditional energy stability holds for the scheme (3.10). We shall prove this in the following Theorem 5. Our proof is for the periodic boundary condition, but in principle it applies to the Neumann type as well.

Lemma 4. *Suppose that $\phi,\ \psi : [0,1]\times\mathbb{R}^+ \to \mathbb{R}$ are two periodic functions. If $L(\phi)$ in (3.3) has the convex splitting form $L(\phi) = L_c(\phi) - L_e(\phi)$ given in (3.7). Then*

$$L(\phi) - L(\psi) \le \langle \delta_\phi L_c(\phi) - \delta_\phi L_e(\psi), \phi - \psi\rangle_{L^2},$$

where $\delta_\phi L_c$ and $\delta_\phi L_e$ represent the first order variational derivatives of L_c and L_e with respect to ϕ, respectively.

Proof. The proof is standard (cf. Theorem 1.1 in [35]). Let

$$\boldsymbol{\phi} = (\phi, \partial_x\phi, \partial_{xx}\phi) \in \mathbb{R}^3,$$
$$\boldsymbol{\psi} = (\psi, \partial_x\psi, \partial_{xx}\psi) \in \mathbb{R}^3,$$

and write

$$L_c(\phi) = \int_0^1 l_c(\phi, \partial_x\phi, \partial_{xx}\phi)\,dx = \int_0^1 l_c(\boldsymbol{\phi})\,dx.$$

According to Property 3, $l_c(\boldsymbol{\phi})$ is convex in all of its arguments, so by the definition of convexity, we get

$$l_c(\boldsymbol{\psi}) - l_c(\boldsymbol{\phi}) \ge \nabla_{\boldsymbol{\phi}} l_c(\boldsymbol{\phi})\cdot(\boldsymbol{\psi}-\boldsymbol{\phi}), \quad \forall \boldsymbol{\phi},\boldsymbol{\psi}\in\mathbb{R}^3. \tag{3.11}$$

Integrating (3.11) gives

$$\begin{aligned} L_c(\psi) - L_c(\phi) \ge \int_0^1 \Big\{ &\partial_\phi l_c(\boldsymbol{\phi})(\psi-\phi) + \partial_{\partial_x\phi} l_c(\boldsymbol{\phi})(\partial_x\psi - \partial_x\phi) \\ &+ \partial_{\partial_{xx}\phi} l_c(\boldsymbol{\phi})(\partial_{xx}\psi - \partial_{xx}\phi)\Big\}\,dx \\ = \langle \delta_\phi L_c(\phi), \psi-\phi\rangle_{L^2}&. \end{aligned} \tag{3.12}$$

The last equality is due to the integration by parts. The similar analysis for $L_e(\phi)$ by exchanging ϕ and ψ shows that

$$L_e(\phi) - L_e(\psi) \ge \langle \delta_\phi L_e(\psi), \phi-\psi\rangle_{L^2}. \tag{3.13}$$

Adding (3.12) and (3.13) yields

$$L(\psi) - L(\phi) \ge \langle \delta_\phi L_c(\phi) - \delta_\phi L_e(\psi), \psi-\phi\rangle_{L^2},$$

i.e.,

$$L(\phi) - L(\psi) \le \langle \delta_\phi L_c(\phi) - \delta_\phi L_e(\psi), \phi-\psi\rangle_{L^2}.$$

□

Theorem 5. *Suppose that $\phi,\ \phi_x,\ \phi_{xxx}$ are periodic. If the energy functional $F(\phi)$ has the convex splitting form $F = F_c - F_e$, then the time-discrete scheme (3.10) is unconditionally energy stable, meaning that for any time step size $\Delta t > 0$, we have*

$$L(\phi^{n+1}) \le L(\phi^n), \quad n = 0,1,2,\cdots,$$

in each k-th cycle.

Proof. From (3.10), we have $\phi^{n+1}-\phi^n=-\Delta t\,\mu^{n+1}$, where $\mu^{n+1}=\delta_\phi L_c(\phi^{n+1})-\delta_\phi L_e(\phi^n)$. Setting $\phi=\phi^{n+1},\ \psi=\phi^n$ in Lemma 4, we have

$$\begin{aligned} L(\phi^{n+1})-L(\phi^n) &\le \langle \delta_\phi L_c(\phi^{n+1})-\delta_\phi L_e(\phi^n),\ \phi^{n+1}-\phi^n\rangle_{L^2} \\ &= \langle \mu^{n+1}, -\Delta t\,\mu^{n+1}\rangle_{L^2} \\ &= -\Delta t\|\mu^{n+1}\|_{L^2}^2 \\ &\le 0, \quad \forall n\ge 0. \end{aligned}$$

□

3.2. **Avoid the time-implicit nonlinear term and construct the linear system.** In many cases, several convex splitting forms for F may be found. Assume $F(\phi)$ has two forms of convex splitting belonging to the following two different classes:

$$F(\phi)=F_c^{\mathrm{l}}(\phi)-F_e^{\mathrm{n}}(\phi), \tag{3.14}$$

and

$$F(\phi)=\widetilde{F}_c^{\mathrm{n}}(\phi)-\widetilde{F}_e^{\mathrm{l}}(\phi), \tag{3.15}$$

where the superscripts "l" and "n" mean that the first order variational derivative is linear or nonlinear in ϕ, respectively. Accordingly, two convex splitting schemes exist to solve the gradient flow $\frac{\partial\phi}{\partial t}=-\frac{\delta F}{\delta\phi}$:

$$\frac{\phi^{n+1}-\phi^n}{\Delta t}=-\frac{\delta F_c^{\mathrm{l}}}{\delta\phi}(\phi^{n+1})+\frac{\delta F_e^{\mathrm{n}}}{\delta\phi}(\phi^n), \tag{3.16}$$

and

$$\frac{\phi^{n+1}-\phi^n}{\Delta t}=-\frac{\delta \widetilde{F}_c^{\mathrm{n}}}{\delta\phi}(\phi^{n+1})+\frac{\delta \widetilde{F}_e^{\mathrm{l}}}{\delta\phi}(\phi^n). \tag{3.17}$$

Both of them satisfy the unconditional energy stability. The difference between (3.16) and (3.17) is that how the nonlinear terms are handled. It is clear that the scheme (3.16) is time-explicit in nonlinear term and hence a linear system is solved to generate ϕ^{n+1} at the next time level. But the scheme (3.17) requires to solve a nonlinear equation for ϕ^{n+1} and so it is not as favorite as (3.16) in general.

In the context of the saddle point problem considered here, our proposed convex splitting scheme for the saddle point problem faces the same difficulty of possible emergence of nonlinear time-implicit term. Actually, if only one convex splitting form like (3.14) or (3.15) is available, then the convex splitting form of the auxiliary functional L defined by (3.8) and (3.9) inevitably runs into this trouble. Either L_c in (3.8) or L_e in (3.9) includes both F_c and F_e, which leads to the appearance of at least one nonlinear term at the implicit time level. However, if one has both (3.14) and (3.15), then this difficulty can be circumvented by combining them together. Take $\alpha,\beta\ge 0$ as an example again. Substituting (3.14) into the first and the third terms on the right hand side of (3.3) and substituting (3.15) into the second and the fourth terms on the right hand side of (3.3), then we have the following

decomposition of L

$$\begin{aligned}
L(\phi) &= F_c^{\mathrm{l}}(\phi) - F_e^{\mathrm{n}}(\phi) - \alpha\big[\widetilde{F}_c^{\mathrm{n}}(\phi) - \widetilde{F}_e^{\mathrm{l}}(\phi)\big] \\
&\quad + \alpha\big[F_c^{\mathrm{l}}(\phi-\tilde{\phi}) - F_e^{\mathrm{n}}(\phi-\tilde{\phi})\big] - \beta\big[\widetilde{F}_c^{\mathrm{n}}(\phi^{(k)}+\tilde{\phi}) - \widetilde{F}_e^{\mathrm{l}}(\phi^{(k)}+\tilde{\phi})\big] \\
&= \Big[F_c^{\mathrm{l}}(\phi) + \alpha\widetilde{F}_e^{\mathrm{l}}(\phi) + \alpha F_c^{\mathrm{l}}(\phi-\tilde{\phi}) + \beta\widetilde{F}_e^{\mathrm{l}}(\phi^{(k)}+\tilde{\phi})\Big] \\
&\quad - \Big[F_e^{\mathrm{n}}(\phi) + \alpha\widetilde{F}_c^{\mathrm{n}}(\phi) + \alpha F_e^{\mathrm{n}}(\phi-\tilde{\phi}) + \beta\widetilde{F}_c^{\mathrm{n}}(\phi^{(k)}+\tilde{\phi})\Big] \\
&=: L_c(\phi) - L_e(\phi),
\end{aligned}$$

where $\tilde{\phi} = (v^{(k+1)} \otimes v^{(k+1)})(\phi - \phi^{(k)})$. It is easy to see that both L_c and L_e are convex with respect to ϕ. The proof is exactly the same as that for Property 3. Theorem 5 in Section 3.1 also holds true in this case.

In summary, the semi-discrete scheme for (3.5) by using the two forms of convex splitting of $F(\phi)$, (3.14) and (3.15), has the following expression:

$$\frac{\phi^{n+1}-\phi^n}{\Delta t} = -\left[\frac{\delta L_c}{\delta\phi}\right]^{n+1} + \left[\frac{\delta L_e}{\delta\phi}\right]^{n}, \tag{3.18}$$

where

$$\begin{aligned}
\left[\frac{\delta L_c}{\delta\phi}\right]^{n+1} &= \frac{\delta F_c^{\mathrm{l}}}{\delta\phi}(\phi^{n+1}) + \alpha\frac{\delta\widetilde{F}_e^{\mathrm{l}}}{\delta\phi}(\phi^{n+1}) \\
&\quad + \beta(v^{(k+1)}\otimes v^{(k+1)})\frac{\delta\widetilde{F}_e^{\mathrm{l}}}{\delta\phi}\Big(\phi^{(k)} + (v^{(k+1)}\otimes v^{(k+1)})(\phi^{n+1}-\phi^{(k)})\Big) \\
&\quad + \alpha(I - (v^{(k+1)}\otimes v^{(k+1)}))\frac{\delta F_c^{\mathrm{l}}}{\delta\phi}\Big(\phi^{n+1} - (v^{(k+1)}\otimes v^{(k+1)})(\phi^{n+1}-\phi_k)\Big), \\
\left[\frac{\delta L_e}{\delta\phi}\right]^{n} &= \frac{\delta F_e^{\mathrm{n}}}{\delta\phi}(\phi^{n}) + \alpha\frac{\delta\widetilde{F}_c^{\mathrm{n}}}{\delta\phi}(\phi^{n}) \\
&\quad + \beta(v^{(k+1)}\otimes v^{(k+1)})\frac{\delta\widetilde{F}_c^{\mathrm{n}}}{\delta\phi}\Big(\phi^{(k)} + (v^{(k+1)}\otimes v^{(k+1)})(\phi^{n}-\phi^{(k)})\Big) \\
&\quad + \alpha(I - (v^{(k+1)}\otimes v^{(k+1)}))\frac{\delta F_e^{\mathrm{n}}}{\delta\phi}\Big(\phi^{n} - (v^{(k+1)}\otimes v^{(k+1)})(\phi^{n}-\phi^{(k)})\Big),
\end{aligned}$$

$n = 0, 1, 2, \ldots,$ and the initial value $\phi^0 = \phi^{(k)}$.

It is easy to see that $\left[\frac{\delta L_c}{\delta\phi}\right]^{n+1}$ is linear and $\left[\frac{\delta L_e}{\delta\phi}\right]^{n}$ is nonlinear. So the scheme (3.18) indeed corresponds to a linear system.

3.3. **Quadratic convergence rate of the IMF for the periodic boundary condition.** In the end of this section, we show the quadratic convergence rate of the IMF in the spatially-extended system when the periodic boundary condition is imposed. This deserves some discussion because the periodic boundary condition will make the index-1 saddle point $\phi^*(\cdot)$ *degenerate*: $\phi^*(\cdot + c)$ is also an index-1 point for any $c \in \mathbb{R}$. In terms of the eigenvalues, a zero eigenvalue arises due to this translation invariance. So the spectrum of the index-1 saddle point has the pattern of $\{\lambda_1 < 0 = \lambda_2 < \lambda_3 < \ldots\}$, which does not satisfy the condition in Theorem 1. We need some extra arguments to supplement the proof of Theorem 1 in [13] when the periodic condition $\phi(0) = \phi(1)$ is imposed. The reader may refer to [13] for the

non-degenerate case to understand some elements in our proof. For the practical issue due to this translation invariance, refer to our discussion in Section 4.3.

Let $\mathcal{M}_p \subset \mathcal{M}$ be the subspace satisfying the period boundary condition at $x = 0$ and 1. Our interest is the index-1 saddle point of the energy functional F in $\mathcal{M}_p$. For any real number c, define the shift operator $\phi \to \theta_c\phi$ in the space $\mathcal{M}_p$

$$\theta_c\phi\,(x) := \phi(x + c).$$

This actually defines an equivalence class. The error then should be defined as the distance from the current state ϕ to the equivalence class of any given true solution $\phi^* \in \mathcal{M}_p$ by

$$e := \min_{c\in\mathbb{R}} \|\phi - \theta_c\phi^*\|\,. \tag{3.19}$$

Note that F satisfies $F(\phi) = F(\theta_c\phi)$ and the inner products, L^2 or H^{-1}, in $\mathcal{M}_p$ also satisfy $\langle\phi, \psi\rangle = \langle\theta_c\phi, \theta_c\psi\rangle$ for all $\phi, \psi \in \mathcal{M}_p$ and $c \in \mathbb{R}$. Then the following theorem holds. We leave the proof in the Appendix.

Theorem 6. *Assume all the eigenvalues of the Hessian at the index-1 saddle point ϕ^* are $\lambda_1 < 0 = \lambda_2 < \lambda_3 \le \dots$ and the zero eigenvalue λ_2 is simple, which corresponds to the only eigenfunction $\partial_x\phi^*$ arising from the translation invariance in space, then the conclusions of Theorem 1, in particular, the local quadratic convergence rate of the mapping Φ, are still true in the periodic function space $\mathcal{M}_p$.*

4. Applications to Ginzburg-Landau free energy

In this section, we apply our method to the Ginzburg-Landau free energy on $[0, 1]$,

$$F(\phi) = \int_0^1 \Big[\frac{\kappa^2}{2}(\frac{\partial\phi}{\partial x})^2 + f(\phi)\Big]\,dx, \tag{4.1}$$

where $\phi(x)$ is an order parameter representing for example the concentration of one of the component in a binary alloy. The mobility parameter $\kappa > 0$. The first term in the free energy is the interface energy and the second term is the bulk energy which has a double well form $f(\phi) = (\phi^2 - 1)^2/4$.

If we consider the gradient flow of F in the $L^2([0, 1])$ space with the standard L^2 inner product $\langle\cdot\,,\cdot\rangle_{L^2}$, then we obtain the (non-conserved) Allen-Cahn (AC) equation

$$\frac{\partial\phi}{\partial t} = -\frac{\delta F}{\delta\phi}(\phi) = \kappa^2\Delta\phi - f'(\phi) = \kappa^2\Delta\phi - (\phi^3 - \phi), \tag{4.2}$$

where $\Delta = \partial_{xx}$. If the gradient flow is defined in the H^{-1} metric $\langle\cdot\,,\cdot\rangle_{H^{-1}}$, then the (conserved) Cahn-Hilliard (CH) equation

$$\frac{\partial\phi}{\partial t} = \Delta\frac{\delta F}{\delta\phi} = -\kappa^2\Delta^2\phi + \Delta(\phi^3 - \phi) \tag{4.3}$$

is obtained.

We are interested in the unstable index-1 saddle point of the Ginzburg-Landau free energy (4.1). These saddle points correspond to the "spike-like" stationary solutions, or "canonical nuclei" discussed in [3]. Similarly to the AC and CH equations, which arise in L^2 metric and H^{-1} metric, respectively, we search for the saddle points of F both in L^2 and in H^{-1} metrics. The calculations of transition states and transition rates for the CH equation have already been done in [40, 26] by using the string method ([8]) and the GAD([10]). We use these two equations as test examples for our new method based on the convex splitting idea.

The boundary conditions we explore include the Neumann type and the periodic type. The Neumann boundary condition is $\partial_x\phi(0) = \partial_x\phi(1) = 0$ for the AC equation and $\partial_x\phi(0) = \partial_x\phi(1) = \partial_x^3\phi(0) = \partial_x^3\phi(1) = 0$ for the CH equation. The periodic boundary condition simply means that $\phi(x) = \phi(x+1),\ \forall x \in [0,1]$, and it produces a degeneracy for any stationary solution corresponding to the invariance of the translation in the spatial variable $\phi(x) \to \phi(x+c)$. This means that the second smallest eigenvalue of the index-1 saddle points is zero. The degeneracy from the periodic boundary condition, however, does not affect the result of the IMF; see Section 3.3 for details. It is also noted that the mass $\int_0^1 \phi(x)dx$ is conservative in H^{-1} metric and thus any stationary solution is still stationary if an arbitrary constant is added, i.e., $\phi(x) \to \phi(x) + c$. This degeneracy can be eliminated simply by restricting the solutions in the space where the value of the mass is chosen beforehand; for the same reason, any eigenvectors or perturbations should thus be restricted to having zero mass. More details will be shown later for this point. The existence of a simple index-1 saddle point under Neumann boundary condition, corresponding to the AC or CH equation, is theoretically guaranteed for sufficient small κ for the double well potential. We refer the reader to [2, 3] and references therein. We restrict our calculation to the case of not too large domain, i.e., the parameter κ in (4.1) is not too small, but small enough to posses saddle points. For the multi-nucleation case in a large domain, refer to works such as [15] for theoretical results.

Now we start to discuss how to apply our new method in Section 3 to this saddle point search problem. In the IMF, the auxiliary functional L given by (3.3) (setting $\alpha = 0$, $\beta = 2$) is

$$L(\phi; \phi^{(k)}, v^{(k+1)}) = F(\phi) - 2F(\hat{\phi}) \tag{4.4}$$

with

$$\hat{\phi} := \phi^{(k)} + \tilde{\phi} = \phi^{(k)} + (v^{(k+1)} \otimes v^{(k+1)})(\phi - \phi^{(k)}), \tag{4.5}$$

where the tensor form $(v \otimes v)u := \langle v, u\rangle v, \forall u, v$, is associated with either L^2 metric or H^{-1} metric. So the formal notation $\langle \cdot\,, \cdot \rangle$ means either $\langle \cdot\,, \cdot \rangle_{L^2}$ (AC–type) or $\langle \cdot\,, \cdot \rangle_{H^{-1}}$ (CH–type).

Next, we give several convex splitting forms of $F(\phi)$ as specified in (3.14) and (3.15). The convex splitting form $F(\phi) = \widetilde{F}_c^{\rm n} - \widetilde{F}_e^{\rm l}$ can be taken as

$$\widetilde{F}_c^{\rm n}(\phi) = \int_0^1 \left[\frac{\kappa^2}{2}(\frac{\partial\phi}{\partial x})^2 + \frac{1}{4}\phi^4 + \frac{1}{4}\right] dx, \quad \widetilde{F}_e^{\rm l}(\phi) = \int_0^1 \frac{1}{2}\phi^2\, dx, \tag{4.6}$$

and for the splitting form $F(\phi) = F_c^{\rm l} - F_e^{\rm n}$, we propose two possibilities:

$$F_{c1}^{\rm l}(\phi) = \int_0^1 \left[\frac{\kappa^2}{2}(\frac{\partial\phi}{\partial x})^2 + \phi^2 + \frac{1}{4}\right] dx, \quad F_{e1}^{\rm n}(\phi) = \int_0^1 -\frac{1}{4}\phi^4 + \frac{3}{2}\phi^2\, dx, \tag{4.7}$$

and

$$F_{c2}^{\rm l}(\phi) = \int_0^1 \left[\frac{\kappa^2}{2}(\frac{\partial\phi}{\partial x})^2 + \frac{5}{2}\phi^2 + \frac{1}{4}\right] dx, \quad F_{e2}^{\rm n}(\phi) = \int_0^1 -\frac{1}{4}\phi^4 + 3\phi^2\, dx. \tag{4.8}$$

Note that these functionals are all convex in the region $\phi \in [-1, 1]$.

4.1. **Saddle points in L^2 metric.**

4.1.1. *The schemes.* In this part, we want to locate the transition state of $F(\phi)$ in L^2 metric. As we mentioned earlier, the gradient flow in this L^2 metric corresponds to the AC equation (4.2). The second-order variational operator $\mathbf{H}(\phi)$ of the energy functional F, evaluated at ϕ, is

$$\mathbf{H}(\phi)\psi = \delta_\phi^2 F\,\psi = -\kappa^2\Delta\psi + f''(\phi)\psi,\ \forall\psi \in H^2([0,1]),$$

where H^2 is the standard Soblev space. The eigenvalue problem for this operator is defined by

$$\mathbf{H}(\phi)\psi = -\kappa^2\Delta\psi + f''(\phi)\psi = \lambda\psi, \tag{4.9}$$

subject to boundary conditions, where λ is the eigenvalue. By the standard result of the Rayleigh quotient, the eigen-pair for the min-mode, denoted by $\{\lambda_1, \psi_1\}$, solves the variational problem

$$\min_{\psi\in H^1([0,1])} \mathcal{R}(\psi) := \frac{\langle\psi, \mathbf{H}\psi\rangle_{L^2}}{\|\psi\|_{L^2}^2} = \frac{\int_0^1 \kappa^2\left|\nabla\psi\right|^2 + f''(\phi)\psi^2\,dx}{\int_0^1 \left|\psi\right|^2 dx}.$$

After the min-mode is obtained, the subproblem of minimizing the auxiliary functional (4.4) is then solved by evolving the gradient flow

$$\frac{\partial\phi}{\partial t} = -\frac{\delta L}{\delta\phi}(\phi) = -\frac{\delta F}{\delta\phi}(\phi) + 2(v\otimes v)\frac{\delta F}{\delta\phi}(\hat{\phi}),$$

i.e.,

$$\frac{\partial\phi}{\partial t} = \kappa^2\Delta\phi - \phi^3 + \phi - 2(v\otimes v)(\kappa^2\Delta\hat{\phi} - \hat{\phi}^3 + \hat{\phi}), \tag{4.10}$$

where the tensor is defined by $(v\otimes v)u := \langle v, u\rangle_{L^2} v,\ \forall v, u$. Note that here $v = v^{(k+1)}$ is the min-mode of $\mathbf{H}(\phi^{(k)})$. $\hat{\phi}$ is defined in (4.5).

Then the numerical schemes based on the convex splitting forms of $F(\phi)$ following (4.6)–(4.8) are constructed as follows.

Convex Splitting Scheme 1. If we apply (4.6) and (4.7) to the convex splitting form of $L(\phi)$, then

$$L(\phi) = \left[F_{c1}^{\mathrm{l}}(\phi) + 2\,\widetilde{F}_e^{\mathrm{l}}(\hat{\phi})\right] - \left[F_{e1}^{\mathrm{n}}(\phi) + 2\,\widetilde{F}_c^{\mathrm{n}}(\hat{\phi})\right] =: L_c(\phi) - L_e(\phi),$$

where

$$\begin{aligned} L_c(\phi) &= \int_0^1 \left[\frac{\kappa^2}{2}\left|\phi_x\right|^2 + \phi^2 + \frac{1}{4} + \hat{\phi}^2\right] dx, \\ L_e(\phi) &= \int_0^1 \left[-\frac{1}{4}\phi^4 + \frac{3}{2}\phi^2 \ + \kappa^2\left|\hat{\phi}_x\right|^2 + \frac{1}{2}\hat{\phi}^4 + \frac{1}{2}\right] dx. \end{aligned}$$

The first order variational derivatives of $L_c(\phi)$ and $L_e(\phi)$ are

$$\begin{aligned} \delta_\phi L_c(\phi) &= -\kappa^2\Delta\phi + 2\phi + 2(v\otimes v)\hat{\phi}, \\ \delta_\phi L_e(\phi) &= -\phi^3 + 3\phi + 2(v\otimes v)\left(-\kappa^2\Delta\hat{\phi} + \hat{\phi}^3\right). \end{aligned}$$

Therefore, the first convex splitting scheme for (4.10) is

$$\begin{aligned} \frac{\phi^{n+1}-\phi^n}{\Delta t} =& \left[\kappa^2\Delta\phi - 2\phi - 2(v\otimes v)\phi\right]^{n+1} \\ &+ \left[-\phi^3 + 3\phi + 2(v\otimes v)\big(-\kappa^2\Delta\hat{\phi} + \hat{\phi}^3\big)\right]^n, \end{aligned} \tag{4.11}$$

by using $\langle v, v\rangle_{L^2} = 1$ and $(v\otimes v)\hat{\phi} = (v\otimes v)\phi$.

Convex Splitting Scheme 2. If we apply (4.6) and (4.8) to the convex splitting form of $L(\phi)$, then

$$L(\phi) = \left[F_{c2}^{\mathrm{l}}(\phi) + 2\,\widetilde{F}_{e}^{\mathrm{l}}(\hat{\phi})\right] - \left[F_{e2}^{\mathrm{n}}(\phi) + 2\,\widetilde{F}_{c}^{\mathrm{n}}(\hat{\phi})\right] =: L_c(\phi) - L_e(\phi),$$

where

$$L_c(\phi) = \int_0^1 \frac{\kappa^2}{2}\left|\phi_x\right|^2 + \frac{5}{2}\phi^2 + \frac{1}{4} + \hat{\phi}^2\,dx,$$
$$L_e(\phi) = \int_0^1 -\frac{1}{4}\phi^4 + 3\phi^2 + \kappa^2\left|\hat{\phi}_x\right|^2 + \frac{1}{2}\hat{\phi}^4 + \frac{1}{2}\,dx,$$

and the first order variational derivatives of $L_c(\phi)$ and $L_e(\phi)$ are

$$\delta_\phi L_c(\phi) = -\kappa^2\Delta\phi + 5\phi + 2\,(v\otimes v)\,\hat{\phi},$$
$$\delta_\phi L_e(\phi) = -\phi^3 + 6\phi + 2(v\otimes v)\left(-\kappa^2\Delta\hat{\phi} + \hat{\phi}^3\right).$$

Therefore, the second convex splitting scheme for (4.10) is

$$\begin{aligned}\frac{\phi^{n+1}-\phi^n}{\Delta t} = &\left[\kappa^2\Delta\phi - 5\phi - 2(v\otimes v)\phi\right]^{n+1} \\ &+ \left[-\phi^3 + 6\phi + 2(v\otimes v)\left(-\kappa^2\Delta\hat{\phi} + \hat{\phi}^3\right)\right]^{n}.\end{aligned} \tag{4.12}$$

Non-convex-splitting Scheme. We need a traditional semi-implicit scheme, which is not in the form of convex splitting, as the benchmark to compare with our convex splitting method. We choose the following one which uses the implicit time level only for the diffusion term

$$\frac{\phi^{n+1}-\phi^n}{\Delta t} = \left[\kappa^2\Delta\phi\right]^{n+1} + \left[\phi - \phi^3 - 2(v\otimes v)\phi + 2(v\otimes v)\left(-\kappa^2\Delta\hat{\phi} + \hat{\phi}^3\right)\right]^{n}. \tag{4.13}$$

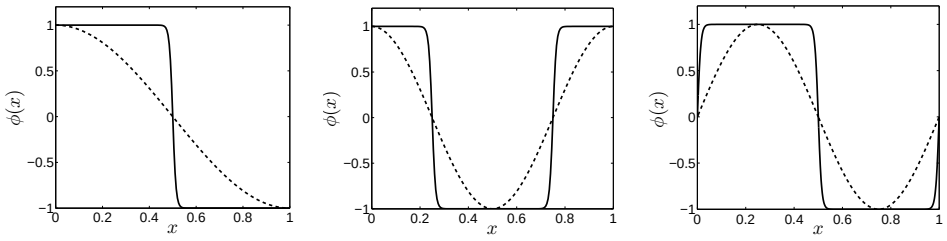

(a) **(b)** **(c)**

FIGURE 1. Profiles of some saddle points (solid lines) of $F(\phi)$ in L^2 metric computed from various initial states (dashed lines). **(a)(b)**: the Neumann boundary condition; **(c)**: the periodic boundary condition. The free energy F for these three plotted states from left to right are 0.0094, 0.0188 and 0.0188, respectively. $\kappa = 0.01$.

4.1.2. *The results.* The finite difference method is used for spatial discretization with the mesh grid $\{x_i = ih, i = 0, 1, 2, \ldots, N\}$. $h = 1/N$. $N = 200$. A finer mesh with $N = 1000$ is also used to verify all numerical results. Set the parameter $\kappa = 0.01$. There are only two locally stable states of the energy potential $F(\phi)$ in L^2 metric regardless of the Neumann or periodic boundary condition. They are the two homogeneous constant states: $\phi_+(x) \equiv 1$ and $\phi_-(x) \equiv -1$. For the Neumann boundary condition, Figure 1a and Figure 1b show the transition states calculated from the convex splitting scheme (4.11) with the initial conditions $\phi_0(x) = \cos \pi x$ and $\phi_0(x) = \cos 2\pi x$, respectively. The second state shown in Figure 1b has two transition layers and its free energy is the double of the one in Figure 1a with a single layer. For the periodic boundary condition, Figure 1c shows the transition state obtained from the initial condition $\phi_0(x) = \sin 2\pi x$, which looks almost identical to the one in Figure 1b after a simple spatial translation.

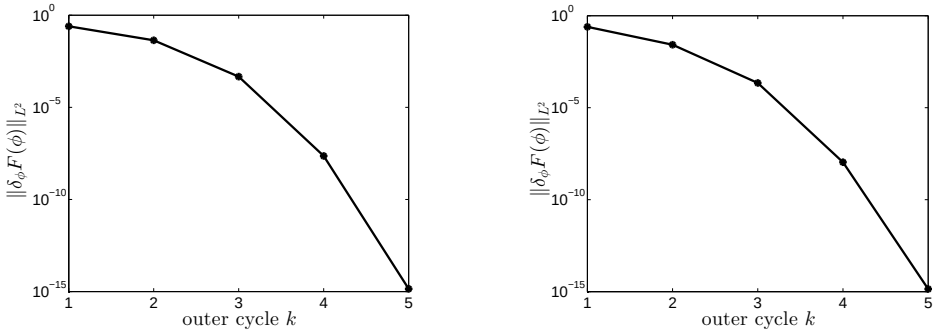

(a) Neumann boundary condition

(b) Periodic boundary condition

FIGURE 2. The validation of the quadratic convergence rate of the IMF mapping Φ by plotting the decay of the error, measured by the force $\|\delta_\phi F(\phi^{(k)})\|_{L^2}$ at each cycle k.

Next we present the numerical evidence on the performance of our numerical method. We first validate the quadratic convergence rate of the IMF for both boundary conditions. In doing this validation which only cares about the rate of the mapping $\phi \to \Phi(\phi)$, we actually deal each subproblem with an extremely high precision. The numerical results are presented in Figure 2 and are consistent with Theorem 1 and Theorem 6.

Now we compare the performance of the convex splitting ("CS") schemes (4.11) and (4.12) against the non-convex splitting ("nCS") scheme (4.13). Firstly, we examine their performance for the subproblem, i.e., within a fixed cycle where only the inner iteration is running. Take the first cycle for example. This is to solve $\min_\phi L(\phi; \phi^{(0)}, v^{(1)})$ with the initial $\phi(t = 0) = \phi^{(0)}$. We measure the error by the gradient force $err := \|\delta_\phi L(\phi^n)\|_{L^2}$. In this cycle, we calculate the iteration number required to attain the given error tolerance for the two CS schemes (4.11) (4.12) and the nCS scheme (4.13). The tolerances we tested are the following three values: $err \le 1.0 \times 10^{-4}, err \le 1.0 \times 10^{-6}$ and $err \le 1.0 \times 10^{-8}$; see Table 1. We can observe from Table 1 for this simple subproblem that (1) the CS schemes obviously have much better stability than the nCS scheme when the time step size is large (∞

The required number of iterations									
Δt	$err = 10^{-4}$			$err = 10^{-6}$			$err = 10^{-8}$		
	(4.11)	(4.12)	(4.13)	(4.11)	(4.12)	(4.13)	(4.11)	(4.12)	(4.13)
0.01	777	799	761	1092	1124	1070	1407	1448	1379
0.95	23	47	59	33	65	101	43	84	145
1	23	46	4801	33	65	9138	42	84	13475
5	16	40	∞	23	56	∞	30	73	∞
10	14	39	∞	21	55	∞	28	71	∞

(a) Neumann boundary condition. The initial state is $\phi^{(0)} = \cos \pi x$.

The required number of iterations						
Δt	$err = 10^{-4}$		$err = 10^{-6}$		$err = 10^{-8}$	
	(4.11)	(4.13)	(4.11)	(4.13)	(4.11)	(4.13)
0.01	728	713	1043	1022	1358	1331
1.0	21	1221	31	2206	41	3191
5.0	14	∞	22	∞	29	∞

(b) Periodic boundary condition. The initial state is $\phi^{(0)} = \sin 2\pi x$.

TABLE 1. The comparison of the CS and nCS schemes for the subproblem within the first cycle $\phi^{(0)} \to \phi^{(1)} = \Phi(\phi^{(0)})$. The integers shown in the table are the required number of iterations for the CS schemes (4.11) and (4.12) as well as the nCS (4.13) to achieve the three choices of the prescribed error tolerance $\|\delta_\phi L(\phi^n)\|_{L^2} \leq 10^{-4}, 10^{-6}$ and 10^{-8}.

in this table means that the numerical results simply diverge); (2) the CS schemes require a less number of iterations (i.e., the time steps) than the nCS scheme to attain the same accuracy and this gain is more significant for the larger time step size; (3) among the two CS schemes we tested, (4.11) seems to work better than the (4.12) in this particular case. The difference between the CS schemes and the nCS scheme is also illustrated in Figure 3, showing that the nCS (4.13) will generate the oscillations, rather than decrease the objective value, when the time step size is larger than 0.95.

Secondly, we provide the numerical evidence for the outperformance of the CS schemes by showing the comparison of the overall efficiency in locating the saddle point. To be more transparent, we fix the number of iterations in each cycle and count the required number of the outer cycles to reach some prescribed tolerance for the error which is defined as $\left\|\delta_\phi F(\phi^{(k)})\right\|_{L^2}$. The comparison is made between the CS scheme (4.11) and the nCS scheme (4.13). The results are summarized in Table 2. The total iteration number, which is the indicator of the total computational cost, is therefore equal to the number of cycles multiplied by the "iter#" specified in the corresponding columns of Table 2. The key conclusions from this table, for both Neumann and periodic boundary conditions, are the following: (1) the gain in the total cost reduction from the CS scheme against the nCS scheme becomes greater when the time step size Δt increases, especially when Δt passes 0.95, regardless of how many "iter#" used in the cycles; (2) for the CS scheme, the larger the time step size is, the smaller the total computational cost is; (3) for the very small time

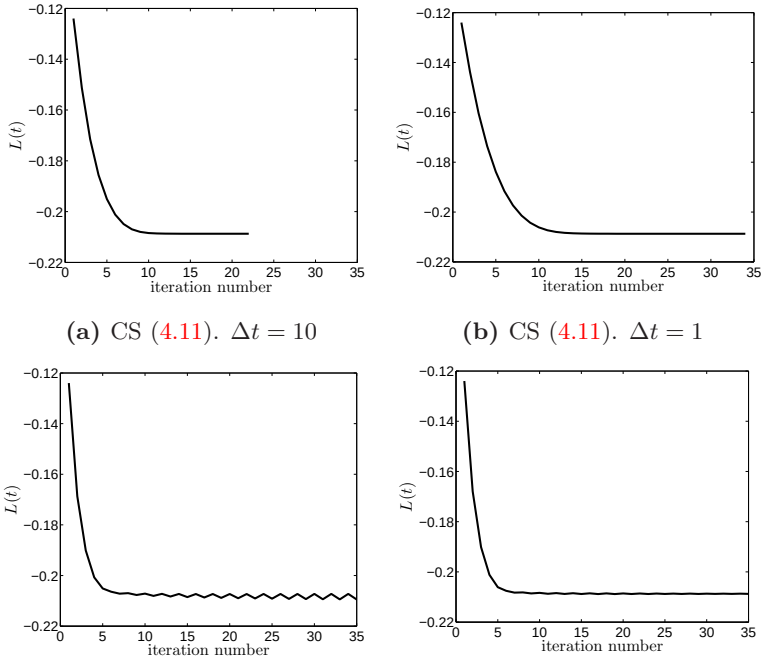

(a) CS (4.11). $\Delta t = 10$ **(b)** CS (4.11). $\Delta t = 1$

(c) nCS (4.13). $\Delta t = 1$ **(d)** nCS (4.13). $\Delta t = 0.95$

FIGURE 3. The numerical value of the objective function $L(\phi(t); \phi^{(0)})$ at time $t_n = n\Delta t$ until *err* is smaller than 10^{-6}. Neumann boundary condition is applied.

step size such as 0.01, there is no much difference in the CS and nCS schemes. Besides, it is also interesting to see that for this particular problem, the total cost seems indifferent to the various values of "iter#".

To better visualize the improvement of the CS scheme over the nCS scheme, we draw the decay of the error $\|\delta_\phi F(\phi)\|_{L^2}$ with respect to the total iteration number in Figure 4. This plot illustrates how much accuracy one can obtain (the vertical axis) with the available total computational cost (the horizontal axis), in which the solid lines are from the CS scheme and the dashed lines are from the nCS scheme.

4.2. **Saddle points in H^{-1} metric.**

4.2.1. *The schemes.* In this part, we study the transition state of $F(\phi)$ in H^{-1} metric. Note that for the convenience of computation, the inner product and the norm in H^{-1} metric can be transformed to those in L^2 metric

$$\|\phi\|_{H^{-1}}^2 = \left\langle (-\Delta)^{-1}\phi, \phi \right\rangle_{L^2}, \ \langle \phi, \psi \rangle_{H^{-1}} = \left\langle (-\Delta)^{-1}\phi, \psi \right\rangle_{L^2}, \tag{4.14}$$

where $(-\Delta)^{-1}$, a bounded positive self-adjoint linear operator, is the inverse of $-\Delta$ subject to certain boundary condition. Then the variational derivatives between the L^2 metric and the H^{-1} metric can be linked as follows:

$$\delta_\phi F\Big|_{H^{-1}} = -\Delta \delta_\phi F, \quad \widetilde{\mathbf{H}} := \delta_\phi^2 F\Big|_{H^{-1}} = -\Delta \delta_\phi^2 F,$$

The number of cycles								
Δt	iter# $= 1$		iter# $= 10$		iter# $= 30$		iter# $= 50$	
	(4.11)	(4.13)	(4.11)	(4.13)	(4.11)	(4.13)	(4.11)	(4.13)
0.01	1408	1380	141	138	47	46	29	28
0.95	45	145	5	15	2	5	1	3
1.0	44	13475	5	1348	2	450	1	270
5.0	34	∞	4	∞	2	∞	1	∞

(a) Neumann boundary condition. The initial state is $\phi^{(0)} = \cos \pi x$.

The number of cycles								
Δt	iter# $= 1$		iter# $= 10$		iter# $= 30$		iter# $= 50$	
	(4.11)	(4.13)	(4.11)	(4.13)	(4.11)	(4.13)	(4.11)	(4.13)
0.01	1359	1332	136	134	46	45	28	27
1.0	43	3191	5	320	2	107	1	64
5.0	33	∞	4	∞	2	∞	1	∞

(b) Periodic boundary condition. The initial state is $\phi^{(0)} = \sin 2\pi x$.

TABLE 2. The comparison of the required number of outer cycles for the CS scheme (4.11) and the nCS scheme (4.13) to attain the given error tolerance $\|\delta_\phi F(\phi^{(k)})\|_{L^2} \le 10^{-8}$ when the inner iteration number is fixed as 1, 10, 30 and 50, respectively, for different choices of the time step size.

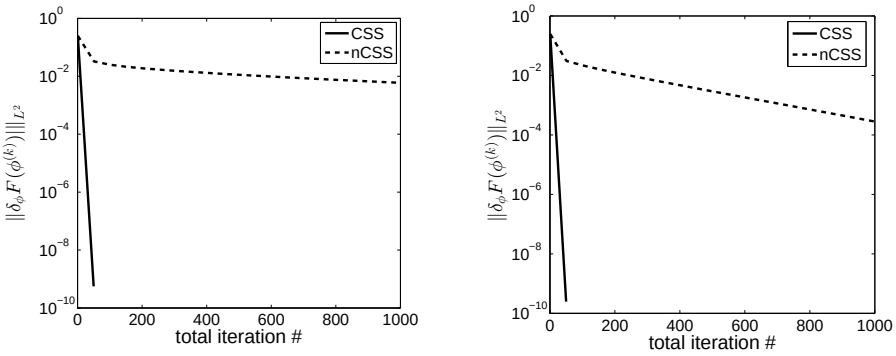

(a) Neumann boundary condition **(b)** Periodic boundary condition

FIGURE 4. The decay of the error measured by the gradient $\|\delta_\phi F(\phi^{(k)})\|_{L^2}$ with the total iteration number (i.e., the cost) for the CS scheme (4.11) (solid line) and the nCS scheme (4.13) (dashed line). The iteration number in each cycle is fixed as 50. The time step size $\Delta t = 1.0$.

where $\delta_\phi F$ and $\delta_\phi^2 F$ represent respectively the first and the second order variational derivatives of $F(\phi)$ in L^2 metric.

The gradient flow $\partial_t \phi = -(-\Delta \delta_\phi F) = -\kappa^2 \Delta^2 \phi + \Delta(\phi^3 - \phi)$ is the CH equation (4.3). It is known that the H^{-1} metric preserves the mass so that the solution

$\phi(x,t)$ of the CH equation (4.3) satisfies $\int_0^1 \phi(x,t)dx \equiv \int_0^1 \phi(x,0)dx, \forall t > 0$, while this property does not hold for the AC equation (4.2). In our problem of finding the saddle point in the H^{-1} metric, we choose a fixed mass m beforehand ($m = 0.6$ in all of our numerical examples), and we are interested in the saddle points satisfying $\int_0^1 \phi(x)dx = m$. For the same reason, we also require any eigenvectors or perturbations to belong to the subspace $\left\{\psi : \int_0^1 \psi(x)dx = 0\right\}$. The eigenvalue problem of $\widetilde{\mathbf{H}}$ is

$$\begin{cases} \widetilde{\mathbf{H}}(\phi)\psi = -\Delta(-\kappa^2\Delta\psi + f''(\phi)\psi) = \lambda\psi, \\ \int_0^1 \psi(x)\,dx = 0, \end{cases} \tag{4.15}$$

subject to the Neumann or periodic boundary condition. For nonzero eigenvalue, the eigenvector ψ automatically satisfies $\int_0^1 \psi dx = 0$; For zero eigenvalue, the condition $\int_0^1 \psi dx = 0$ needs to be imposed additionally. If we introduce the projection $\mathbf{P}u := u - \int_0^1 u(x)\,dx$, then the eigen-problem (4.15) is equivalent to $\mathbf{P}\widetilde{\mathbf{H}}\mathbf{P}u = \lambda u$ for any u without the mass constraint. The min-mode is then equal to u if the eigenvalue is nonzero and equal to $\mathbf{P}u$ if the eigenvalue is zero.

For the periodic boundary condition where $\phi(x) = \phi(x+1)$ for all x, there exists one degenerate ($\lambda = 0$) direction ψ_0 for the Hessian $\widetilde{\mathbf{H}}(\phi)$, which is the spatial derivative of ϕ, i.e.,

$$\psi_0(x) = \phi_x(x).$$

To see this, we just need verify (4.15) by using the periodic boundary condition: $\int_0^1 \phi_x(x)dx = \phi(1) - \phi(0) = 0$ and

$$\int_0^1 -\Delta(-\kappa^2\Delta\phi_x + f''(\phi)\phi_x)dx = \int_0^1 \kappa^2\partial_x^5\phi(x) - \partial_x^2(\partial_x(f'(\phi(x))))\ dx = 0.$$

In fact, this degenerate direction comes from the translation invariance for the energy functional $F(\phi) = F(\phi_c)$, where $\phi_c(x) = \phi(x+c)$ for any $c \in \mathbb{R}$. Refer to Section 3.3 and the appendix for more general discussions.

The Rayleigh quotient with respect to H^{-1} metric is

$$\widetilde{\mathcal{R}}(\psi) = \frac{\left\langle \psi, \widetilde{\mathbf{H}}\psi \right\rangle_{H^{-1}}}{\|\psi\|_{H^{-1}}^2} = \frac{\int_0^1 \kappa^2 \left|\nabla\psi\right|^2 + f''(\phi)\psi^2\,dx}{\int_0^1 \psi\Delta^{-1}\psi dx},$$

and thus the min-mode is the minimizer of the problem

$$\operatorname*{argmin}_{\psi} \left\{ \widetilde{\mathcal{R}}(\psi) : \int_0^1 \psi\,dx = 0,\ \|\psi\|_{H^{-1}} = 1 \right\}. \tag{4.16}$$

For the IMF in the context of this H^{-1} case, the subproblem of minimizing the auxiliary functional L for a given $\phi^{(k)}$ at cycle k is

$$\phi^{(k+1)} = \operatorname*{argmin}_{\int_0^1 \phi(x)dx = m} L(\phi; \phi^{(k)}, v^{(k+1)}), \tag{4.17}$$

where $m = \int_0^1 \phi^{(k)}dx$. This means that each IMF cycle $\phi^{(k)} \to \phi^{(k+1)}$ should also conserve the mass. We shall show that this constraint is guaranteed for the H^{-1} gradient flow of L.

The expression of $L(\phi)$ is defined as (4.4), with the modification of $\hat{\phi}$ as follows

$$\begin{aligned}\hat{\phi} &:= \phi^{(k)} + \left\langle v, \phi - \phi^{(k)} \right\rangle_{H^{-1}} v = \phi^{(k)} + \left\langle -\Delta^{-1} v, \phi - \phi^{(k)} \right\rangle_{L^2} v \\ &= \phi^{(k)} + \left\langle w, \phi - \phi^{(k)} \right\rangle_{L^2} v,\end{aligned} \tag{4.18}$$

where

$$w := -\Delta^{-1} v$$

is the unique solution satisfying the equation $-\Delta w = v$ and the additional condition $\int_0^1 w\, dx = 0$. Then,

$$\delta_\phi L(\phi) = \delta_\phi F(\phi) - 2w \left\langle \delta_\phi F(\hat{\phi}), v \right\rangle_{L^2},$$

and the H^{-1} gradient flow of L is

$$\frac{\partial \phi}{\partial t} = \Delta \frac{\delta L}{\delta \phi}(\phi) = \Delta \left(\frac{\delta F}{\delta \phi}(\phi) \right) + 2v \left\langle \frac{\delta F}{\delta \phi}(\hat{\phi}), v \right\rangle_{L^2}, \tag{4.19}$$

i.e.,

$$\frac{\partial \phi}{\partial t} = -\kappa^2 \Delta^2 \phi + \Delta(\phi^3 - \phi) + 2v \left\langle v, -\kappa^2 \Delta \hat{\phi} + \hat{\phi}^3 - \hat{\phi} \right\rangle_{L^2}, \tag{4.20}$$

where $v = v^{(k+1)}$ refers to the min-mode of (4.15) at $\phi^{(k)}$ (normalized under H^{-1} metric, i.e., $\|v\|_{H^{-1}} = 1$). $\frac{\delta F}{\delta \phi}(u) = -\kappa^2 \Delta u + f'(u)$ is the L_2 gradient of F at u. Note that the scalar in the second term on the right hand side of (4.19) is actually the L^2 inner product due to the cancelation of Δ and Δ^{-1} in the calculation, but the variable $\hat{\phi}$ does involve the H^{-1} metric. This suggests one more computational cost of solving $w = -\Delta^{-1} v$ during the IMF subproblem than the GAD scheme where $\hat{\phi}$ is actually just $\phi^{(k)}$ and only one step solution is used ([14]). Our result (4.19) is consistent with the equation (3.4) in [26] which was written for the GAD in the finite dimension, i.e., $\hat{\phi} = \phi^{(k)}$. Here in the IMF, $\hat{\phi}$ also changes as ϕ in (4.19) marches with time in the subproblem.

Remark 1. *We show that the flow* (4.19) *conserves the initial mass* $\int_0^1 \phi(x)dx$, *sharing exactly the same property as the CH equation* (4.3). *So the constraint in* (4.17) *holds automatically. This result immediately implies that the IMF mapping* $\phi^{(k)} \to \phi^{(k+1)}$ *does not change the mass at each cycle* k. *To prove our conclusion, after integrating the two sides of* (4.19) *and using the boundary conditions (either Neumann or periodic), one remains to show the following condition for the eigenvector* v: $\int_0^1 v(x)dx = 0$. *This is exactly the condition that the min-mode* v *satisfies in* (4.15).

Next we present some numerical details on the schemes.

Convex splitting scheme. We only test the convex splitting form of (4.6)–(4.7); that is,

$$L(\phi) = L_c(\phi) - L_e(\phi),$$

where

$$L_c(\phi) = F_{c1}^l(\phi) + 2\tilde{F}_e^l(\hat{\phi}), \quad L_e(\phi) = F_{e1}^n(\phi) + 2\tilde{F}_c^n(\hat{\phi}),$$

and $\hat{\phi}$ is defined in (4.18). Then simple calculations show that

$$\delta_\phi L_c(\phi) = -\kappa^2\Delta\phi + 2\phi + 2\left\langle v, \hat{\phi}\right\rangle_{L^2} w,$$
$$\delta_\phi L_e(\phi) = -\phi^3 + 3\phi + 2\left\langle -\kappa^2\Delta\hat{\phi} + \hat{\phi}^3, v\right\rangle_{L^2} w.$$

Thus the convex splitting scheme for (4.19) is for $n = 0, 1, 2, \ldots$

$$\begin{aligned}\frac{\phi^{n+1}-\phi^n}{\Delta t} = &\left[-\kappa^2\Delta^2\phi^{n+1} + 2\Delta\phi^{n+1} - 2\left\langle w, \phi^{n+1}\right\rangle_{L^2}\langle v, v\rangle_{L^2} v\right] \\ &- 2\left\langle v, \phi^{(k)}\right\rangle_{L^2} v + 2\left\langle w, \phi^{(k)}\right\rangle_{L^2}\langle v, v\rangle_{L^2} v \\ &+ \left[\Delta(\phi^n)^3 - 3\Delta\phi^n + 2\left\langle v, -\kappa^2\Delta\hat{\phi}^n + (\hat{\phi}^n)^3\right\rangle_{L^2} v\right],\end{aligned} \tag{4.21}$$

where $v = v^{(k+1)}$, $w = -\Delta^{-1}v^{(k+1)}$ and $\hat{\phi}^n$ is from (4.18) by letting $\phi = \phi^n$. On the right hand side of this CS scheme (4.21), the first line is linear in the unknown ϕ^{n+1}, the second line is independent of n, the third line is the nonlinear term in ϕ^n.

Non-convex splitting scheme. The non-convex splitting finite difference scheme is similar to the one used for the L^2 metric in Section 4.1, which uses the implicit time level for the term $\Delta^2\phi$

$$\frac{\phi^{n+1}-\phi^n}{\Delta t} = -\kappa^2\left[\Delta^2\phi\right]^{n+1} + \left[\Delta\phi^3 - \Delta\phi + 2\left\langle v, -\kappa^2\Delta\hat{\phi} + \hat{\phi}^3 - \hat{\phi}\right\rangle_{L^2} v\right]^n. \tag{4.22}$$

We set the mesh grid $\{x_i = ih, i = 0, 1, 2, \ldots, N\}$. $h = 1/N$. $N = 200$. The parameter $\kappa = 0.04$. The function $\phi(x)$ is represented by $\boldsymbol{\phi} = (\phi_0, \phi_1, \phi_2, \cdots, \phi_N)^T$ for the Neumann boundary condition and $\boldsymbol{\phi} = (\phi_0, \phi_1, \phi_2, \cdots, \phi_{N-1})^T$ for the periodic boundary condition; $\phi_i \approx \phi(x_i)$. The matrix form of the Hessian $\widetilde{\mathbf{H}}$ at the state $\boldsymbol{\phi}$ is

$$\widetilde{\mathbf{H}}(\boldsymbol{\phi}) = A\nabla^2 F_h(\boldsymbol{\phi}),$$

where $\nabla^2 F_h(\boldsymbol{\phi}) = \frac{\partial^2 F_n}{\partial\phi_i\partial\phi_j}$. A and $F_h(\boldsymbol{\phi})$ denote the discretized forms of the operator $-\Delta$ and the potential energy $F(\phi)$, respectively. For the Neumann boundary condition,

$$A = \frac{1}{h^2}\begin{pmatrix} 1 & -1 & 0 & \cdots & 0 & 0 \\ -1 & 2 & -1 & 0 & \cdots & 0 \\ 0 & \ddots & \ddots & \ddots & \ddots & 0 \\ 0 & 0 & \cdots & -1 & 2 & -1 \\ 0 & 0 & \cdots & 0 & -1 & 1 \end{pmatrix} \in \mathbb{R}^{(N+1)\times(N+1)},$$

and

$$F_h(\boldsymbol{\phi}) = \frac{\kappa^2}{2}\sum_{i=1}^{N}\left(\frac{\phi_i - \phi_{i-1}}{\Delta x}\right)^2\Delta x + \left[\sum_{i=1}^{N-1} f(\phi_i) + \frac{1}{2}f(\phi_0) + \frac{1}{2}f(\phi_N)\right]\Delta x.$$

For the periodic boundary condition,

$$A = \frac{1}{h^2}\begin{pmatrix} 2 & -1 & 0 & \cdots & 0 & -1 \\ -1 & 2 & -1 & 0 & \cdots & 0 \\ 0 & \ddots & \ddots & \ddots & \ddots & 0 \\ 0 & 0 & \cdots & -1 & 2 & -1 \\ -1 & 0 & \cdots & 0 & -1 & 2 \end{pmatrix} \in \mathbb{R}^{N\times N},$$

and

$$F_h(\boldsymbol{\phi}) = \frac{\kappa^2}{2}\sum_{i=1}^{N}\big(\frac{\phi_i - \phi_{i-1}}{\Delta x}\big)^2\Delta x + \sum_{i=0}^{N-1} f(\phi_i)\Delta x, \text{ with } \phi_N = \phi_0.$$

Actually, by (4.15), the equivalent form of $\widetilde{\mathbf{H}}$ is $\kappa^2 A^2 + A\,\mathrm{diag}\,\{f''(\boldsymbol{\phi})\}$. The min-mode v of the Hessian matrix $\widetilde{\mathbf{H}}$ can be calculated according to the Rayleigh quotient (4.16).

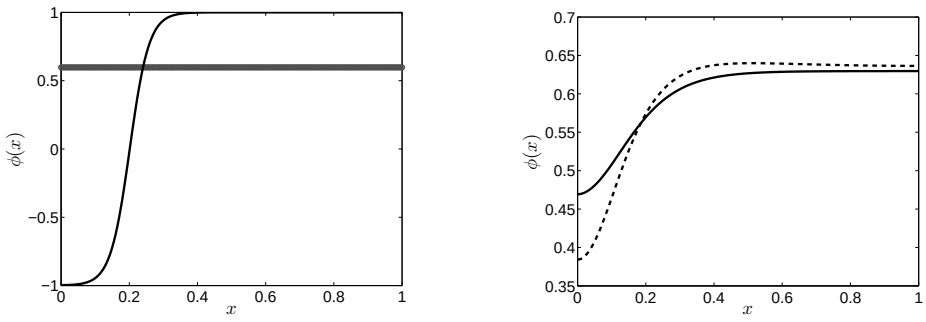

(a) Two locally stable states **(b)** Transition state

FIGURE 5. (Neumann boundary condition. H^{-1} metric.) **(a)**: the two stable stationary states of $F(\phi)$ with the mass $\int_0^1 \phi\,dx = 0.6$. $F = 0.10240$ for the trivial constant state (the thick line) and $F = 0.03772$ for the transition layer state (the thin line). **(b)**: one of the transition states (solid line) with the free energy 0.10241 whose first 3 eigenvalues are $\lambda = -3.41, 3.91$ and 18.14, calculated from the initial condition (dashed line) whose first 3 eigenvalues are $\lambda = -10.97, 3.45$ and 17.48. Note that the vertical axes in subfigures are in different scales.

4.2.2. *The results.* Figure 5 and Figure 6 show some of the stationary states of F in H^{-1} metric for the Neumann and periodic boundary conditions, respectively. The stationary points identified by us agree with the result obtained in [40]. Note that for the Neumann boundary condition case, there are other stationary states by the symmetric mirror $\phi(x) \to \phi(1-x)$ or with higher index, which are not shown in our figures. Similarly to Figure 2 for the AC-type saddle point, Figure 7 validates the quadrate convergence rate of the IMF again for this H^{-1} case. The error is

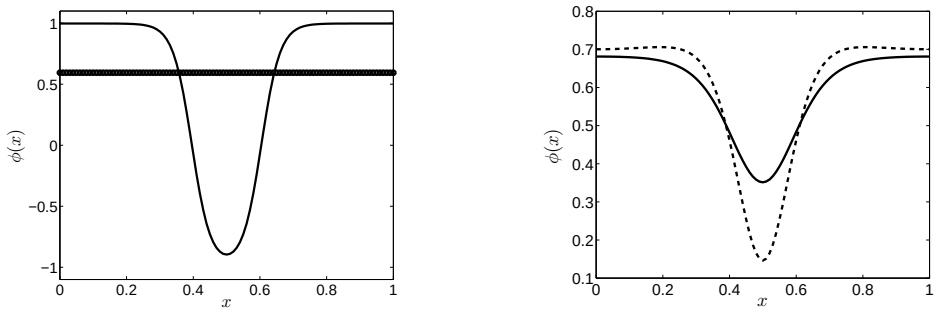

(a) Two locally stable states **(b)** Transition state

FIGURE 6. (Periodic boundary condition. H^{-1} metric.) **(a)**: the two stable stationary states of $F(\phi)$ in H^{-1} metric with the given mass $\int_0^1 \phi\, dx = 0.6$. $F = 0.10240$ for the constant state and $F = 0.07510$ for the other non-constant state. **(b)**: one of the transition states (solid line) with the free energy 0.10285 whose first three smallest (numerical) eigenvalues are $-12.75, -1.86 \times 10^{-7}$ (corresponding to theoretical zero eigenvalue) and 46.15. The initial state is shown as the dashed line in which the first 3 smallest eigenvalues are $\lambda = -27.13, -6.81$ and 44.98. $\kappa = 0.04$. Note the different scales in the vertical axes.

measured by the force in H^{-1} metric:

$$err := \left\| \delta_\phi F(\phi^{(k)})|_{H^{-1}} \right\|_{H^{-1}} = \left\| -\Delta \delta_\phi F(\phi^{(k)}) \right\|_{H^{-1}}$$
$$= \left(\left\langle \delta_\phi F(\phi^{(k)}), -\Delta \delta_\phi F(\phi^{(k)}) \right\rangle_{L^2} \right)^{1/2}.$$

Next we make comparison for the performance of the CS scheme (4.21) and the nCS shceme (4.22). We also start from their performance for the subproblem. Take the first cycle for example. We compare the number of inner iterations required for (4.21) and (4.22) with various time step sizes to attain the error tolerances of minimizing L in the first cycle. So the stopping criteria is $\|\Delta \delta_\phi L\|_{H^{-1}} \le 1.0 \times 10^{-4}, 1.0 \times 10^{-5}$ or 1.0×10^{-6}, respectively. Table 3 shows the comparison results. We can observe from Table 3 that (1) the CS scheme has a much better stability than the nCS scheme for large time step sizes in both Neumann and the periodic boundary conditions; (2) when both the CS and nCS schemes have convergence for a small time step size, the nCS scheme may require a less number of the iterations to reach the tolerance, in particular for the periodic boundary condition. This is possible because a scheme with a better stability does not guarantee a faster convergence rate toward the minimum. What matters here in this table is that a larger time step size requires a much less number of iterations, which is numerically valid for both the CS and nCS schemes, provided that the results converge.

The advantage of applying a large time step size in the CS scheme is furthermore demonstrated by checking the overall efficiency of the CS scheme (4.21) and nCS scheme (4.22). Similarly to the AC-type problem, with the number of inner iteration being fixed, the required number of cycles for the error $\|\Delta \delta_\phi F(\phi^{(k)})\|_{H^{-1}}$ to achieve

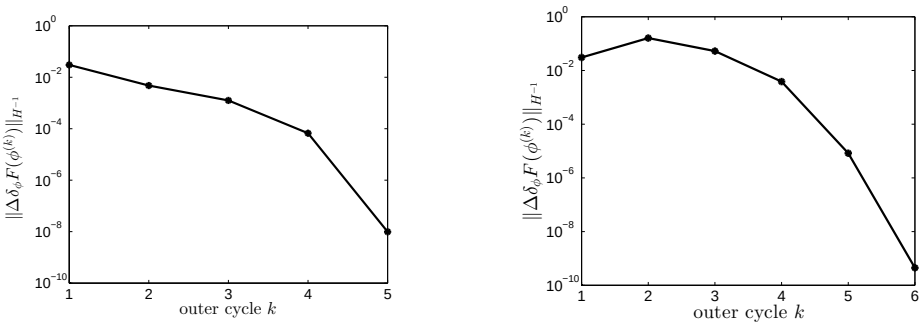

(a) Neumann boundary condition

(b) Periodic boundary condition

FIGURE 7. The validation of the quadratic convergence rate of the IMF mapping by plotting the decay of the error, measured by the H^{-1} norm of the H^{-1} gradient, i.e., $\|\Delta\delta_\phi F(\phi)\|_{H^{-1}}$ at each cycle k. The corresponding initial states are specified in Figure 5b and 6b, respectively.

The required number of iterations						
Δt	$err = 10^{-4}$		$err = 10^{-5}$		$err = 10^{-6}$	
	(4.21)	(4.22)	(4.21)	(4.22)	(4.21)	(4.22)
10^{-3}	2956	2653	3332	2999	3709	3346
10^{-2}	550	∞	617	∞	685	∞
10^{-1}	283	∞	321	∞	360	∞
1.0	14	∞	262	∞	298	∞

(a) Neumann boundary condition.

The required number of iterations						
Δt	$err = 10^{-4}$		$err = 10^{-5}$		$err = 10^{-6}$	
	(4.21)	(4.22)	(4.21)	(4.22)	(4.21)	(4.22)
10^{-3}	1022	838	1163	957	1305	1076
10^{-2}	281	97	316	109	351	121
10^{-1}	208	∞	233	∞	257	∞

(b) Periodic boundary condition.

TABLE 3. The comparison of the CS scheme (4.21) and nCS scheme (4.22) for the subproblem $\phi^{(0)} \to \phi^{(1)} = \Phi(\phi^{(0)})$. The integers shown in the table are the required number of iterations to achieve the three prescribed tolerances $\|\Delta\delta_\phi L(\phi^n)\|_{H^{-1}} \leq 10^{-4}, 10^{-5}$ and 10^{-6}.

the prescribed tolerances are listed in Table 4. We can read from this table that (1) for a small time step size ($\Delta t = 10^{-3}$) when both schemes converge, the CS scheme and the nCS scheme require nearly the same computational cost; (2) for the CS scheme, the total computational cost decreases significantly when the time

step size increases, especially from 10^{-3} to 10^{-2}; for the nCS scheme, however, it diverges when $\Delta t > 10^{-3}$.

The number of cycles						
Δt	iter# $= 40$		iter# $= 50$		iter# $= 60$	
	CSS	nCSS	CSS	nCSS	CSS	nCSS
10^{-3}	118	103	95	82	79	69
10^{-2}	28	∞	22	∞	16	∞
10^{-1}	16	∞	17	∞	16	∞

(a) Neumann boundary condition.

The number of cycles						
Δt	iter# $= 50$		iter# $= 80$		iter# $= 100$	
	CSS	nCSS	CSS	nCSS	CSS	nCSS
10^{-3}	34	26	22	17	18	14
10^{-2}	13	∞	7	∞	8	∞
10^{-1}	11	∞	8	∞	7	∞

(b) Periodic boundary condition.

TABLE 4. The comparison of the number of outer cycles required for the CS scheme (4.21) and the nCS scheme (4.22) to attain the given error tolerance $\|\Delta\delta_\phi F(\phi^{(k)})\|_{H^{-1}} \leq 10^{-8}$, when the inner iteration number is fixed for the different choices of the time step size $\Delta t = 10^{-3}, 10^{-2}$ and 10^{-1}. The corresponding initial states are specified in Figure 5b and Figure 6b, respectively.

In the end, based on the experiments corresponding to Table 4, we plot the evolution of the error measured by the force $\|\Delta\delta_\phi F(\phi^{(k)})\|_{H^{-1}}$ against the total iteration number (i.e., the cost) for the CS scheme and the nCS scheme by using their own optimal time step sizes respectively. See Figure 8, which is similar to Figure 4 for the case of AC-type problem. Here for the CH-type problem, in order to illustrate that the results are robust with respect to the initial guess, we actually add the random perturbation to generate multiple initial states so that multiple lines are plotted for several different initial guesses.

4.3. **Discussion.** The choice of the initial guess is an important practical issue for all existing numerical methods of calculating the saddle points. The GAD or the IMF only has the local convergence and thus in the extreme case, one can easily construct a very special initial guess which does not have convergence. In addition, the subproblem of minimizing the auxiliary functional is well-defined only when the minimal eigenvalue of the original Hessian is negative; otherwise, it should not be solved thoroughly, but limited to a fixed few number of iterations, such as the GAD. For the readers particularly interested in the practical convergence issue, refer to the discussion in [14]. Most numerical results we reported here are for one typical choice of initial conditions (except for Figure 8), but our unreported numerical experiments by trying various initial guesses, still strongly support the conclusions that a larger time step size means a lower computational cost and that the CS scheme can allow for such large time step sizes.

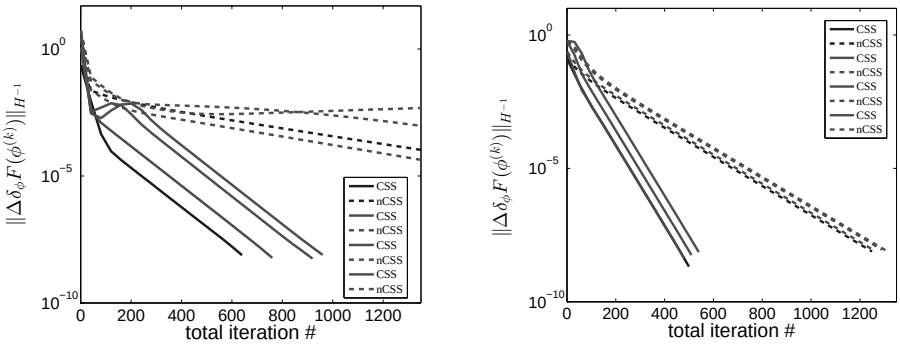

(a) Neumann boundary condition **(b)** Periodic boundary condition

FIGURE 8. The evolution of the errors measured by $\|\Delta\delta_\phi F(\phi)\|_{H^{-1}}$ w.r.t. the total iteration number for the CS scheme (4.21) (solid lines) and the nCS scheme (4.22) (dashed lines). Different small perturbations around the initial condition used in Table 4 are added as the new initial conditions here to produce multiple lines. For the Neumann boundary condition in (**a**), the inner iteration number is 40 and the time step sizes are $\Delta t = 10^{-1}$ and 10^{-3} for the CS and nCS schemes, respectively. For the periodic boundary condition in (**b**), the inner iteration number is 50. The time step sizes are the same as in (**a**).

Finally, we emphasize another critical problem of selecting the correct "min-mode" in the implementation. Generally speaking, the calculation of the min-mode is self-explanatory by minimizing the corresponding Rayleigh quotient. But if one starts from a local minimizer of F, say $\bar{\phi}$, then the eigenvalues at this locally stable state are $\{0 = \lambda_1 < \lambda_2 < \ldots\}$ for the periodic boundary condition and the min-mode is then the zero eigenvector $v_1 = \partial_x\bar{\phi}$ by definition. However, it is quite clear that taking $\partial_x\bar{\phi}$ as the min-mode is a very bad choice since it will not push the state away but only translate the state back and forth around $\bar{\phi}$. This means that the dynamics could converge to a minimizer of F. This pathological case could also appear for certain very special initial states in the convex region of F. For example, it might happen when the minimal eigenvalue λ_1 crosses over zero from positive to negative (from the convex region to the non-convex region), i.e., near the so-called branching point. Even for the Neumann boundary condition, this could also happen if the state happens to satisfy the periodic boundary condition loosely. This phenomena certainly does not contradict with our Theorem 6 which states the local convergence result requiring λ_1 being strictly negative. The remedy to avoid this pathological situation in practice is extremely simple: at a state ϕ, whenever the angle between v_1 and $\partial_x\phi$ is close to 0° or 180° (set by a prescribed threshold in the algorithm), a constraint is added to make sure that the min-mode v in use for the auxiliary functional L must be orthogonal to $\partial_x\phi$. In this way, a strictly positive λ_2 is selected and accordingly, v_2 is selected as the "min-mode" in the pathological case. As long as λ_1 starts to take a negative value, the angle defined above becomes 90° automatically and there is no interference between the

min-mode v_1 and the translation direction $\partial_x\phi$. Thus the constraint becomes in no need at all. After taking care of this issue, we found that almost for all initial guesses we tried, we did observe the convergence of the algorithm to some index-1 saddle point.

5. Conclusion

We have demonstrated how the convex splitting method can improve the efficiency of the transition-state calculation by allowing for the preferred large time step size. For the Ginzburg-Landau energy, this new method has been applied for the first time to find index-1 saddle points of the Allen-Cahn and Cahn-Hilliard types, i.e., under the L_2 and H^{-1} metrics, respectively. The main advantage of using the convex splitting scheme is to avoid the instability when the time step size is large. And it is also very inspiring that our extensive numerical studies in this paper have shown the significant improvement of the computational efficiency. Therefore, for spatially extended systems driven by an energy functional such as the phase field models or the Kohn-Sham density functional ([25]), we have reasons to speculate that many matured and excellent numerical methods for the traditional gradient dynamics may be able to exhibit their new vitalities for saddle point calculation, if they are correctly wrapped by the iterative minimization formulation.

Appendix A. Proof of the quadratic convergence rate of the IMF for the periodic boundary condition

This appendix is devoted for the proof of Theorem 6 in Section 3.3. If a function $\phi \in \mathcal{M}_p$ is a stationary point of F, then the first order variational derivative $\delta_\phi F(\theta_c\phi)$ at ϕ's equivalence class is independent of c. It immediately implies that $H(\phi)\partial_x\phi = 0$ for any $\phi \in \mathcal{M}_p$ by taking the second order derivative in c (see [40]). So we have this lemma:

Lemma 7. *At each stationary state $\phi \in \mathcal{M}_p$, the Hessian has one eigenvector $\partial_x\phi$ for the zero eigenvalue.*

For the stationary point of interest in Theorem 6, it is assumed that the eigenspace of this zero eigenvalue (equivalently, the null space of the Hessian) is one dimensional, i.e., spanned by $\partial_x\phi$.

Lemma 8. *The IMF mapping Φ and the shift operator θ_c commute. This is to say*

$$\Phi \circ \theta_c = \theta_c \circ \Phi, \quad \text{for any } c \in \mathbb{R}. \tag{A.1}$$

Proof. It is easy to show that $F(\phi) = F(\theta_c\phi)$ implies $\theta_c F'(\phi) = F'(\theta_c\phi)$ and $\theta_c \circ H(\phi) = H(\theta_c\phi) \circ \theta_c$, where F' and H are the first and the second order Frechlet derivative of F. Now consider the mapping $\phi \to \Phi(\phi)$. First, look at the min-modes $v(\phi)$ and $v(\theta_c\phi)$ evaluated at ϕ and its shift $\theta_c\phi$, respectively. We claim that $v(\theta_c\phi) = \theta_c v(\phi)$ since $H(\theta_c\phi) \circ \theta_c v = \theta_c \circ H(\phi)v = \theta_c(\lambda v) = \lambda\theta_c v$ for $v = v(\phi)$. It follows from this result that for any ψ and ϕ in $\mathcal{M}_p$,

$$L(\psi; \phi, v) = L(\theta_c\psi; \theta_c\phi, \theta_c v), \tag{A.2}$$

with $v = v(\phi)$, by simply checking the definition of L in (2.3) and using $\langle \cdot, \cdot \rangle = \langle \theta_c \cdot, \theta_c \cdot \rangle$.

To prove the conclusion (A.1), i.e., $\Phi(\theta_c\phi) = \theta_c \circ \Phi(\phi)$, it suffices to show $\theta_c \circ \Phi(\phi)$ is a minimizer of $L(\cdot\,; \theta_c\phi, v(\theta_c\phi))$ or equivalently $L(\cdot\,; \theta_c\phi, \theta_c v)$. So, we just need to show

$$L(\theta_c \circ \Phi(\phi); \theta_c\phi, \theta_c v) \le L(\psi;\ \theta_c\phi, \theta_c v),\ \forall \psi \in \mathcal{M}_p.$$

By (A.2), this is equivalent to show

$$L(\Phi(\phi); \phi, v) \le L(\psi; \theta_c\phi, \theta_c v),\ \forall \psi \in \mathcal{M}_p.$$

Note that by its definition, $\Phi(\phi)$ satisfies

$$L(\Phi(\phi); \phi, v) \le L(\psi'; \phi, v),\ \forall \psi' \in \mathcal{M}_p.$$

By letting $\psi' = \theta_{-c} \circ \psi$ and noting (A.2), we complete the proof. □

Corollary 8.1. *Let $J(\phi) = \nabla\Phi(\phi)$ be the Jacobi of the mapping Φ at $\phi \in \mathcal{M}_p$, then*

$$J(\phi)\partial_x\phi = \partial_x(\Phi(\phi)). \tag{A.3}$$

Particularly, at the saddle point ϕ^* (defined in Theorem 6), we have $\Phi(\phi^*) = \phi^*$, and thus

$$J_*\partial_x\phi^* = \partial_x\phi^*, \tag{A.4}$$

which means that $\partial_x\phi^*$ is a right eigenfunction of $J_* = J(\phi^*)$.

Proof. Since $\partial_x\phi(x) = \lim_{\varepsilon\to 0}\frac{1}{\varepsilon}(\phi(x+\varepsilon) - \phi(x)) = \lim_{\varepsilon\to 0}\frac{1}{\varepsilon}(\theta_\varepsilon \circ \phi(x) - \phi(x))$, then by using Lemma 8 twice, we have

$$\begin{aligned} J(\phi)\partial_x\phi &= \lim_{\varepsilon\to 0}\frac{1}{\varepsilon}(\Phi(\phi + \varepsilon\partial_x\phi) - \Phi(\phi)) \\ &= \lim_{\varepsilon\to 0}\frac{1}{\varepsilon}(\Phi(\theta_\varepsilon\phi) - \Phi(\phi) + \mathcal{O}(\varepsilon^2)) \\ &= \lim_{\varepsilon\to 0}\frac{1}{\varepsilon}(\theta_\varepsilon \circ \Phi(\phi) - \Phi(\phi)) \\ &= \partial_x(\Phi(\phi)), \end{aligned}$$

where $\mathcal{O}(\varepsilon^2)$ means the infinitesimal term of the second order in ε. □

We start to prove Theorem 6.

Proof. We first remark that the error defined in (3.19) is a measurement of the distance from the current state ϕ to the equivalence class of the solution ϕ^*. Now we prove the quadratic convergence rate. Following the derivation in [13] for the proof of Theorem 1, we still have the following property

$$(H_* - 2v_* \otimes v_*)J_*u = 0,\ \forall u \in \mathcal{M}, \tag{A.5}$$

where H_*, v_* and J_* are the Hessian of F, the min-mode and the Jacobi of Φ at ϕ^*, respectively.

By Lemma 7 and noting the orthogonality of the two eigenvectors, i.e., v_* and $\partial_x\phi^*$, corresponding to $\lambda_1 < 0$ and $\lambda_2 = 0$ respectively, we have

$$(H_* - 2v_* \otimes v_*)\partial_x\phi^* = 0,$$

and one can easily show that the null space of $H_* - 2v_* \otimes v_*$ is exactly spanned by $\partial_x\phi^*$. So (A.5) suggests that there exists a scalar α for each $u \in \mathcal{M}_p \subset \mathcal{M}$ such that

$$J_*u = \alpha\partial_x\phi^*.$$

We now write each u as the direct sum $u = u_1 \oplus \beta\partial_x\phi^*$, where u_1 is orthogonal to the null space $\partial_x\phi^*$ and β is a scalar. Then

$$J_*u = J_*u_1 + \beta J_*\partial_x\phi^* = J_*u_1 + \beta\partial_x\phi^*$$

due to (A.4). Therefore

$$J_*u_1 = (\alpha - \beta)\partial_x\phi^*. \tag{A.6}$$

Now we examine the residual at cycle k and show the convergence rate in local sense. For $\phi^{(k)} \in \mathcal{M}_p$ and the next value after this cycle $\phi^{(k+1)} := \Phi(\phi^{(k)})$, we write

$$\varepsilon := \left\|\phi^{(k)} - \phi^*\right\| \quad \text{and} \quad \varepsilon u := \phi^{(k)} - \phi^*,$$

where ϕ^* is already shifted in space according to $\phi^{(k)}$ so that ε is a small number. The function u defined here is thus at order $\mathcal{O}(1)$ and the above discussion is applied to this particular u. We discuss two cases for this u.

Case 1. u satisfies that $\alpha = \beta$ in (A.6), i.e.,

$$J_*u_1 = 0, \tag{A.7}$$

then the error at the $(k+1)$-th cycle then satisfies

$$\begin{aligned}
e_{k+1} &= \min_c \left\|\phi^{(k+1)} - \theta_c\phi^*\right\| = \min_c \left\|\Phi(\phi^{(k)}) - \theta_c\phi^*\right\| \\
&= \min_c \left\|\Phi(\phi^{(k)}) - \Phi(\phi^*) + \phi^* - \theta_c\phi^*\right\| \\
&= \min_c \|\varepsilon J_*u + \phi^* - \theta_c\phi^*\| + \mathcal{O}(\varepsilon^2) \\
&= \min_c \|\varepsilon J_*u_1 + \varepsilon\beta\partial_x\phi^* + \phi^* - \theta_c\phi^*\| + \mathcal{O}(\varepsilon^2),
\end{aligned}$$

where u_1 and β associated with u are defined earlier.

Now by choosing $c = \varepsilon\beta$, we continue to have

$$\begin{aligned}
e_{k+1} &\le \|\varepsilon J_*u_1 + \varepsilon\beta\partial_x\phi^* + (\phi^* - \theta_{\varepsilon\beta}\phi^*)\| + \mathcal{O}(\varepsilon^2) \\
&= \|\varepsilon J_*u_1 + \varepsilon\beta\partial_x\phi^* - \varepsilon\beta\partial_x\phi^*\| + \mathcal{O}(\varepsilon^2) \\
&= \varepsilon\,\|J_*u_1\| + \mathcal{O}(\varepsilon^2),
\end{aligned}$$

where $\theta_c f(x) = f(x+c) = f(x) + c\partial_x f(x) + \mathcal{O}(c^2)$ is applied. By the condition (A.7), $J_*u_1 = 0$, so we have shown $e_{k+1} \sim \mathcal{O}(e_k^2)$.

Case 2. If the assumption in *Case 1* is not true, then $J_*u_1 = \gamma\partial_x\phi^*$, where $\gamma = \alpha - \beta$ is nonzero. The similar argument in *Case 1* for e_{k+1} leads to

$$\begin{aligned}
e_{k+1} &= \min_c \|\varepsilon J_*u_1 + \varepsilon\beta\partial_x\phi^* + \phi^* - \theta_c\phi^*\| + \mathcal{O}(\varepsilon^2) \\
&= \min_c \|\varepsilon\gamma\partial_x\phi^* + \varepsilon\beta\partial_x\phi^* + \phi^* - \theta_c\phi^*\| + \mathcal{O}(\varepsilon^2) \\
&\le \|\varepsilon\alpha\partial_x\phi^* + \phi^* - \theta_{\varepsilon\alpha}\phi^*\| + \mathcal{O}(\varepsilon^2) \\
&= \|\varepsilon\alpha\partial_x\phi^* - \varepsilon\alpha\partial_x\phi^*\| + \mathcal{O}(\varepsilon^2) \\
&= \mathcal{O}(\varepsilon^2),
\end{aligned}$$

which also indicates the quadratic convergence rate. The optimal $c = \varepsilon\alpha$ is used in this case. □

References

[1] Samuel M. Allen and John W. Cahn. A microscopic theory for antiphase boundary motion and its application to antiphase domain coarsening. *Acta Metallurgica*, 27:1085–1095, 1979.

[2] Peter W. Bates and Paul C. Fife. Spectral comparison principles for the Cahn-Hilliard and phase-field equations and time scales for coarsening. *Phys. D*, 43(2-3):335–348, 1990.

[3] Peter W. Bates and Paul C. Fife. The dynamics of nucleation for the Cahn-Hilliard equation. *SIAM J. Appl. Math.*, 53(4):990–1008, 1993.

[4] John W. Cahn and John E. Hilliard. Free energy of a nonuniform system. I. interfacial free energy. *J. Chem. Phys.*, 28(2):258–267, 1958.

[5] E. Cancès, F. Legoll, M.-C. Marinica, K. Minoukadeh, and F. Willaime. Some improvements of the activation-relaxation technique method for finding transition pathways on potential energy surfaces. *J. Chem. Phys.*, 130(11):114711, 2009.

[6] C. J. Cerjan and W. H. Miller. On finding transition states. *J. Chem. Phys.*, 75(6):2800–2806, 1981.

[7] G. M. Crippen and H. A. Scheraga. Minimization of polypeptide energy : XI. the method of gentlest ascent. *Arch. Biochem. Biophys.*, 144(2):462–466, 1971.

[8] W. E, W. Ren, and E. Vanden-Eijnden. String method for the study of rare events. *Phys. Rev. B*, 66:052301, 2002.

[9] W. E, W. Ren, and E. Vanden-Eijnden. Simplified and improved string method for computing the minimum energy paths in barrier-crossing events. *J. Chem. Phys.*, 126:164103, 2007.

[10] W. E and X. Zhou. The gentlest ascent dynamics. *Nonlinearity*, 24(6):1831, 2011.

[11] David J. Eyre. An unconditionally stable one-step scheme for gradient systems. *manuscript, http://www.math.utah.edu/ eyre/research/methods/papers.html*, 1998.

[12] David J. Eyre. Unconditionally gradient stable time marching the Cahn-Hilliard equation. In Jeffrey W. Bullard et al., editors, *Computational and Mathematical Models of Microstructural Evolution*, volume 529, pages 39–46. MRS, Warrendale, PA,1998.

[13] W. Gao, J. Leng, and X. Zhou. An iterative minimization formulation for saddle point search. *SIAM J. Numer. Anal.*, 53(4):1786–1805, 2015.

[14] W. Gao, J. Leng, and X. Zhou. Iterative minimization algorithm for efficient calculations of transition states. *J. Comput. Phys.*, 309:69–87, 2016.

[15] Michael Gelantalis and Maria G. Westdickenberg. Energy barrier and γ-convergence in the d-dimensional Cahn–Hilliard equation. *Calculus of Variations and Partial Differential Equations*, 54(1):791–829, 2015.

[16] S. Gu, H. Zhang, and Z. Zhang. An energy-stable finite-difference scheme for the binary fluid-surfactant system. *J. Comput. Phys.*, 270:416–431, 2014.

[17] G. Henkelman and H. Jónsson. A dimer method for finding saddle points on high dimensional potential surfaces using only first derivatives. *J. Chem. Phys.*, 111(15):7010–7022, 1999.

[18] G. Henkelman and H. Jónsson. Theoretical calculations of dissociative adsorption of CH_4 on an Ir(111) surface. *Phys. Rev. Lett.*, 86(4):664–667, 2001.

[19] G. Henkelman, B. P. Uberuaga, and H. Jónsson. A climbing image nudged elastic band method for finding saddle points and minimum energy paths. *J. Chem. Phys.*, 113(22):9901–9904, 2000.

[20] A. Heyden, A.T. Bell, and F.J. Keil. Efficient methods for finding transition states in chemical reactions: Comparison of improved dimer method and partitioned rational function optimization method. *J. Chem. Phys.*, 123:224101, 2005.

[21] Z. Hu, S.M. Wise, C. Wang, and J.S. Lowengrub. Stable and efficient finite-difference nonlnear-multigrid schemes for the phase field crystal equation. *J. Comp. Phys.*, 228(15):5323–5339, 2009.

[22] H. Jònsson, G. Mills, and K. W. Jacobsen. Nudged elasic band method for finding minimum energy paths of transitions. In B. J. Berne, G. Ciccotti, and D. F. Coker, editors, *Classical and Quantum Dynamics in Condensed Phase Simulations*, page 385, New Jersey, 1998. LERICI, Villa Marigola,Proceedings of the International School of Physics, World Scientific.

[23] J. Kästner and P. Sherwood. Superlinearly converging dimer method for transition state search. *J. Chem. Phys.*, 128:014106, 2008.

[24] J. Leng, W. Gao, C. Shang, and Z.-P. Liu. Efficient softest mode finding in transition states calculations. *J. Chem. Phys.*, 138(9):094110, 2013.

[25] Chen Li, Jianfeng Lu, and Weitao Yang. Gentlest ascent dynamics for calculating first excited state and exploring energy landscape of Kohn-Sham density functionals. *The Journal of Chemical Physics*, 143(22):224110, 2015.

[26] T. Li, P. Zhang, and W. Zhang. Nucleation rate calculation for the phase transition of diblock copolymers under stochastic Cahn–Hilliard dynamics. *Multiscale Modeling & Simulation*, 11(1):385–409, 2013.

[27] R. Malek and N. Mousseau. Dynamics of Lennard-Jones clusters: A characterization of the activation-relaxation technique. *Phys. Rev. E*, 22(6):7723–7728, 2000.

[28] N. Mousseau and G.T. Barkema. Traveling through potential energy surfaces of disordered materials: the activation-relaxation technique. *Phys. Rev. E*, 57:2419, 1998.

[29] J. Nocedal. *Numerical Optimization*. Springer Series in Operations Research. Springer-Verlag, 1999.

[30] R. A. Olsen, G. J. Kroes, G. Henkelman, A. Arnaldsson, and H. Jònsson. Comparison of methods for finding saddle points without knowledge of the final states. *J. Chem. Phys.*, 121(20):9776–9792, 2004.

[31] H. Bernhard Schlegel. Exploring potential energy surfaces for chemical reactions: An overview of some practical methods. *J. Comput. Chem.*, 24(12):1514–1527, 2003.

[32] J. Shen, C. Wang, X. M. Wang, and S.M. Wise. Second-order convex splitting schemes for gradient flows with Ehrlich-Schwoebel type energy: application to thin film epitaxy. *SIAM J. Numer. Anal.*, 50(1):105–125, 2012.

[33] J. Shen and X.F. Yang. Decoupled energy stable schemes for phase-field model of two-phase complex fluids. *SIAM J. SCI. Comput.*, 36(1):B122–B145, 2014.

[34] C. Wang and S.M. Wise. An energy stable and convergent finite-difference scheme for the modified phase field crystal equation. *SIAM J. Numer. Anal.*, 49(3):945–969, 2011.

[35] S. M. Wise, C. Wang, and J.S. Lowengrub. An energy-stable and convergent finite-difference scheme for the phase field crystal equation. *SIAM J. Numer. Anal.*, 47(3):2269–2288, 2009.

[36] S.M. Wise. Unconditionally stable finite difference, nonlinear multigrid simulation of the Cahn-Hilliard-Hele-Shaw system of equations. *J. Sci. Comput*, 44(1):38–68, 2010.

[37] Y. Zeng, P. Xiao, and G. Henkelman. Unification of algorithms for minimum mode optimization. *J. Chem. Phys.*, 140(4):044115, 2014.

[38] J. Zhang and Q. Du. Shrinking dimer dynamics and its applications to saddle point search. *SIAM J. Numer. Anal.*, 50:1899–1921, 2012.

[39] L. Zhang, W. Ren, A. Samanta, and Q. Du. Recent developments in computational modelling of nucleation in phase transformations. *npj Computational Materials*, 2:16003, 2016.

[40] W. Zhang, T. Li, and P. Zhang. Numerical study for the nucleation of one-dimensional stochastic Cahn-Hilliard dynamics. *Comm. Math. Sci.*, 10:1105–1132, 2012.